Characterization of metal flow evolution during indirect extrusion of 6061 aluminum alloy

Browne, Heather M.

Characterization of Metal Flow Evolution During Indirect Extrusion of 6061 Aluminum Alloy

May 2004

Characterization of Metal Flow Evolution During Indirect Extrusion of 6061 Aluminum Alloy

By

Heather M. Browne

A Thesis
Presented to the Graduate and Research Committee
Of Lehigh University
In Candidacy for the Degree of
Master of Science

In

Materials Science and Engineering

Lehigh University
April 30, 2004

CERTIFICATE OF APPROVAL

This thesis is accepted and approved in partial fulfillment of the requirements for the Master of Science.

_____
Date

_____
Wojciech Z. Misiolek
Thesis Advisor

_____
Slade Cargill
Chairperson

ACKNOWLEDGEMENTS

I would like to extend my deepest thanks to the following organizations and individuals without whom this work would not have been possible. First and foremost, I would like to thank the Extrusion Technology for Aluminum Profiles Foundation for providing me with financial support through the first Graduate Student Fellowship. I would like to also thank Dr. Paul Wang and Richard Kelly of Werner Co. for their guidance and knowledge in the development of this thesis. I would like to thank Alcoa for providing me with billet material and the use of their deformation simulator at the Alcoa Technical Center with special thanks to Jacob Kallivayalil and technician for assisting me with my experiments.

I would also like to thank my fellow IMF members whose help, knowledge, and guidance is greatly appreciated. Special thanks to William VanGeertruyden for fruitful discussions, endless EBSD assistance, and constant support and Alex Bandar for his grateful assistance. I would also like to thank undergraduate students Neil Hurley and Mike Guinta for graciously helping me during this terribly straining year. Also, thanks to Arlan Benscoter and Kai Lorchorensary for their metallographic knowledge and assistance, and Dr. Marcelo Goncalves for his advice and assistance. Special thanks to my advisor, Dr. Wojciech Z. Misiolek, whose admirable work ethic, professionalism, and guidance is most appreciated.

Lastly, I would like to thank all the people closest to me for their undying support through my graduate program especially this past year, specifically my

mother Deborah, brother Douglas, grandparents Harold and Gloria, aunt Denise and Royce. This thesis is dedicated to my father, John J. Browne (3/30/51-4/2/04).

TABLE OF CONTENTS

LIST OF TABLES

LIST OF FIGURES

ABSTRACT

Research regarding aluminum extrusion technology is vast in order to understand this widely used forming process. Of wide industrial concern is the existence of surface imperfections, such as Peripheral Coarse Grain (PCG) structure, in aluminum extrudates. This thesis evaluates the microstructural evolution of the billet at the die face during indirect extrusion in order to properly understand the effect of metal flow and microstructural evolution in the billet on final extrudate microstructure, particularly PCG formation.

Small-scale indirect extrusions interrupted at 25, 50, and 75% completion were performed on two variations of AA6061. Metal flow and microstructure evolution was investigated and analyzed using light optical microscopy (LOM) and Electron Backscatter Diffraction (EBSD) techniques. The EBSD technique proved to be the most useful tool in evaluating microstructural development and metal flow on the meso-scale. EBSD results revealed an increase in dead metal zone volume as extrusion progressed from 25% to 75% completion. This increase is proposed to result from the continuing formation and fragmentation of new, high-angle, fine grains along the dead metal/shear zone interface possibly due to a continuous recrystallization process.

1.0 INTRODUCTION

1.1 Aluminum Extrusion Fundamentals

Extrusion is a metal forming process where a billet of material is plastically deformed by being forced through a die opening to produce products of smaller, constant cross sectional area. Commonly extruded materials include, but are not limited to, aluminum, copper, titanium, steel, magnesium, lead and their alloys. Extrusion can be performed at room temperature or elevated temperature depending on the ductility of the material to be extruded. These materials can be extruded to a variety of shapes termed extrudates. Geometries of extrudates can vary from simple shapes such as bars, rods, and round tubes to products with extremely complex geometries. Final product dimensions are dependent upon the geometry of the die utilized.

There are two main types of extrusion: direct and indirect. The direct process involves the billet being forced through the die orifice by an applied ram pressure on the back of the billet. During direct extrusion, the billet moves relative to the container walls causing the extrudate to exit the die in the same direction as the ram displacement. Friction is created at the billet/container and billet/die interfaces during direct extrusion. With the indirect process, the billet remains stationary while the die moves into the billet. Unlike the direct process, the extrudate in indirect extrusion exits the die opposite the direction of ram displacement. Indirect extrusion

is thus characterized by the elimination of friction at the billet-container interface [2, 3]. A schematic of both the direct and indirect processes can be seen in Figure 1.

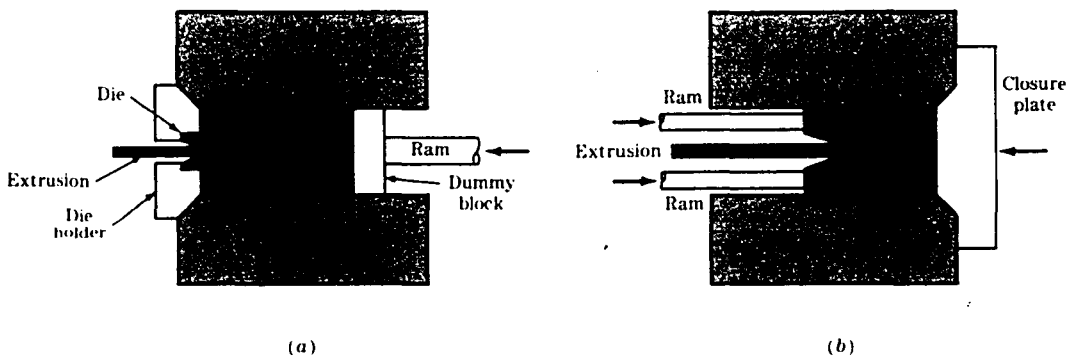

Figure 1: Schematic of (a) direct extrusion process and (b) indirect extrusion process [4]

Extrusion of a material is often defined by numerous geometric variables. Characteristic of most extruded products is their constant cross sectional area as determined by the die geometry. The reduction in cross sectional area from the upset billet to extrudate is termed the extrusion ratio, R, and is commonly used in practice to define the strain during extrusion.

Another crucial parameter is die design. Die angles can greatly influence metal flow through the die orifice during extrusion thus dictating velocity and strain gradients across the extruded product. There are three general die types: a flat face die, conical die, and convex die. A flat face die sits at a 90° angle with the container wall. The metal entering a flat face die will form its own die angle resulting from the

is thus characterized by the elimination of friction at the billet-container interface [2, 3]. A schematic of both the direct and indirect processes can be seen in Figure 1.

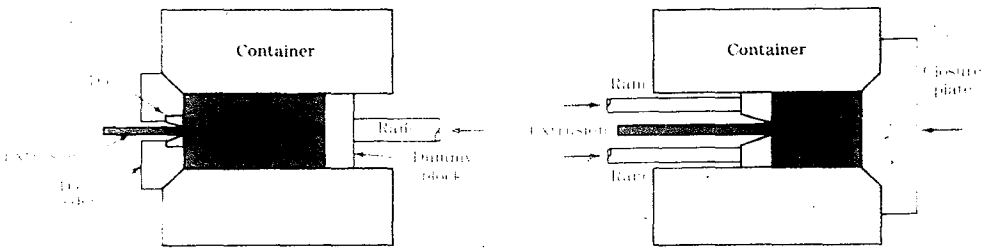

Figure 1: Schematic of (a) direct extrusion process and (b) indirect extrusion process [4]

Extrusion of a material is often defined by numerous geometric variables. Characteristic of most extruded products is their constant cross sectional area as determined by the die geometry. The reduction in cross sectional area from the upset billet to extrudate is termed the extrusion ratio, R, and is commonly used in practice to define the strain during extrusion.

Another crucial parameter is die design. Die angles can greatly influence metal flow through the die orifice during extrusion thus dictating velocity and strain gradients across the extruded product. There are three general die types: a flat face die, conical die, and convex die. A flat face die sits at a 90° angle with the container wall. The metal entering a flat face die will form its own die angle resulting from the

formation of a dead metal zone and shear zone during direct extrusion. Formation of these zones will be discussed in greater detail in following sections. The second type of die design, a conical die, is used in extrusion of copper alloys and steel with good lubrication. A conical die design increases homogeneity of flow into the die orifice thus decreasing the strain gradients across the final product. The third die design is a convex die. The theory behind a convex die is to extend the die angle beyond 90°. As the die angle is extended beyond 90°, the field of radial metal flow entering the die orifice is increased. An increase in radial metal flow leads to a more uniform velocity profile and strain gradient at the die orifice thus leading to a more homogenous final microstructure. Schematics of the three general extrusion dies can be seen in Figure 2.

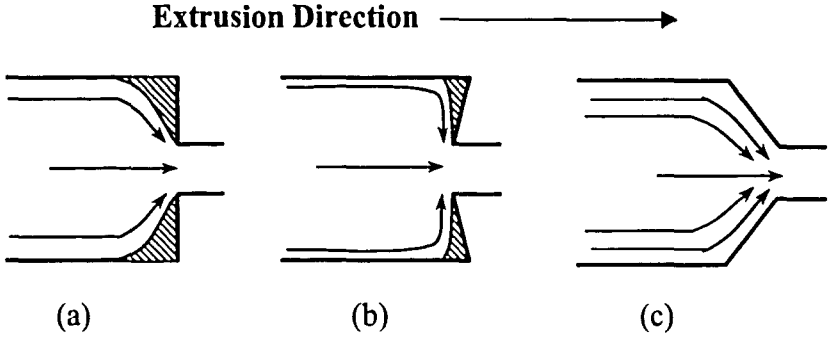

Figure 2: Schematic of general extrusion die types including (a) flat-face die, (b) convex die, and (c) concave die design and resulting dead metal zone formation.

The research presented in this thesis will investigate the effect of various process parameters specifically strain, strain rate, cooling rate, material and

deformation temperature on structure development within the billet during indirect extrusion of 6061 aluminum alloy. Understanding the formation and evolution of deformation zones during extrusion specifically the geometry of dead metal zones is crucial to understanding the development of microstructure frequently witnessed in final extrudates.

1.2 Metal Flow

Various metal flow patterns can result during an extrusion process depending on the extruded material and process employed, direct or indirect. Understanding and predicting metal flow during extrusion is crucial to advancing aluminum extrusion technology. Metal flow dictates the velocity and strain gradients extrudates experience thus largely influencing final microstructure and properties of the extruded product. Numerous flow patterns exist for various materials. Traditional extrusion flow patterns have been detected for metal extrusion using various techniques. Most commonly used techniques to analyze metal flow during extrusion include the grid technique and the use of model material such as lead, wax, or plasticine [5, 6]. Grid techniques require the billet to be sectioned longitudinally such that a grid can be inscribed on the center surfaces as seen in Figure 3. These two faces are placed back together to form the original billet and partially extruded [6]. Deformed grid patterns can then be analyzed for information regarding billet/container and billet/die interactions during extrusion, velocity distributions for particles within the material, and the basic mode of deformation [5]. Physical

simulation using model materials has also contributed significantly to the understanding of metal flow during extrusion. Billets comprised of model materials can be made by varying the color of model material throughout the height of a billet. An example of a partially extruded billet using color variations can be seen in Figure 4. Partial extrusion of model materials, as with the grid technique, can provide information as to the mode of deformation during extrusion.

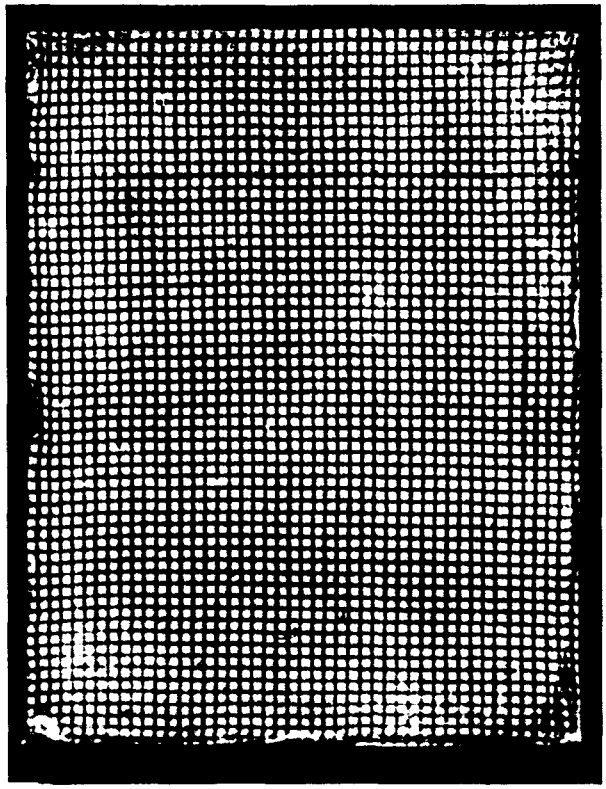

Figure 3: Example of starting billet grid pattern for physical modeling [7].

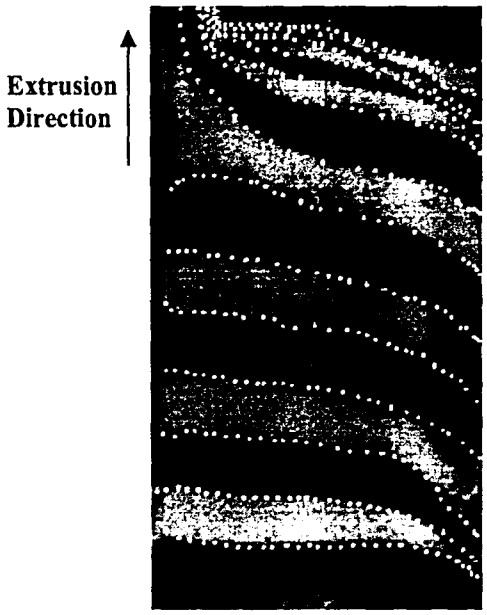

Figure 4: Example of partially extruded plasticine billet [8].

As previously stated, traditional extrusion flow patterns have been extensively studied and are classified into four general types as proposed by Pearson/Dũrrschnabel: S, A, B, and C as seen in Figure 5 [9, 10]. Hot extrusion of aluminum has been found to exhibit two additional intermediary flow types not included in this general classification of extrusion flow [10]. Figure 5 exhibits these two intermediary flow patterns, A_1 and B_1, for indirect and direct extrusion of aluminum respectively with the original classification system.

Extrusion flow patterns within a billet normally exhibit three distinct regions: deformation zone, shear zone, and dead metal zone. These areas within the billet are identified in Figure 5 for indirect and direct extrusion processes. Deformation zones form in the billet near the die face with a depth that varies according to the process

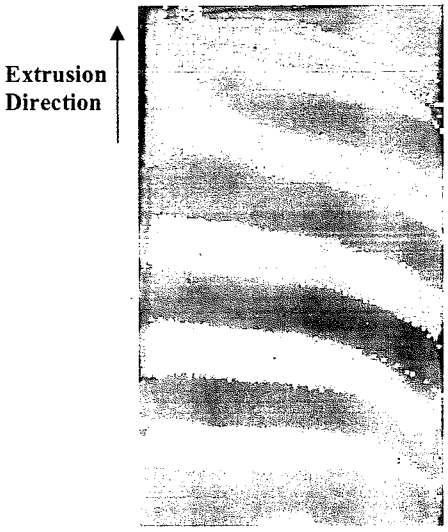

Figure 4: Example of partially extruded plasticine billet [8].

As previously stated, traditional extrusion flow patterns have been extensively studied and are classified into four general types as proposed by Pearson/Dũrrschnabel: S, A, B, and C as seen in Figure 5 [9, 10]. Hot extrusion of aluminum has been found to exhibit two additional intermediary flow types not included in this general classification of extrusion flow [10]. Figure 5 exhibits these two intermediary flow patterns, A_1 and B_1, for indirect and direct extrusion of aluminum respectively with the original classification system.

Extrusion flow patterns within a billet normally exhibit three distinct regions: deformation zone, shear zone, and dead metal zone. These areas within the billet are identified in Figure 5 for indirect and direct extrusion processes. Deformation zones form in the billet near the die face with a depth that varies according to the process

employed. Contained within the deformation zone are both the shear and dead metal zones. The shear zone, as labeled in Figure 5, can be found in both direct and indirect processes where intensive shearing of the material occurs. As extrusion progresses, the shear zone shape and size varies drastically [11]. The shear zone that develops during indirect extrusion varies significantly from that found in direct extrusion as it is concave in shape as can be seen in Figure 5. Dead metal zones are areas of metal that remain stationary during the extrusion process. Dead metal zones typically form in direct extrusion in the area of metal between the die corner and shear zone due to friction at the die/container interface. Dead metal zone formation in indirect extrusion of aluminum has been argued since evidence does exist of metal "leaking" from the dead zone into the extrudate surface as will be discussed later.

The research presented will focus primarily on the metal flow during indirect extrusion of hot aluminum specifically the formation and evolution of a "dead metal zone". Understanding the evolution of dead metal and shear zone geometry during extrusion is of great significance to understanding extrudate microstructures for various processing conditions.

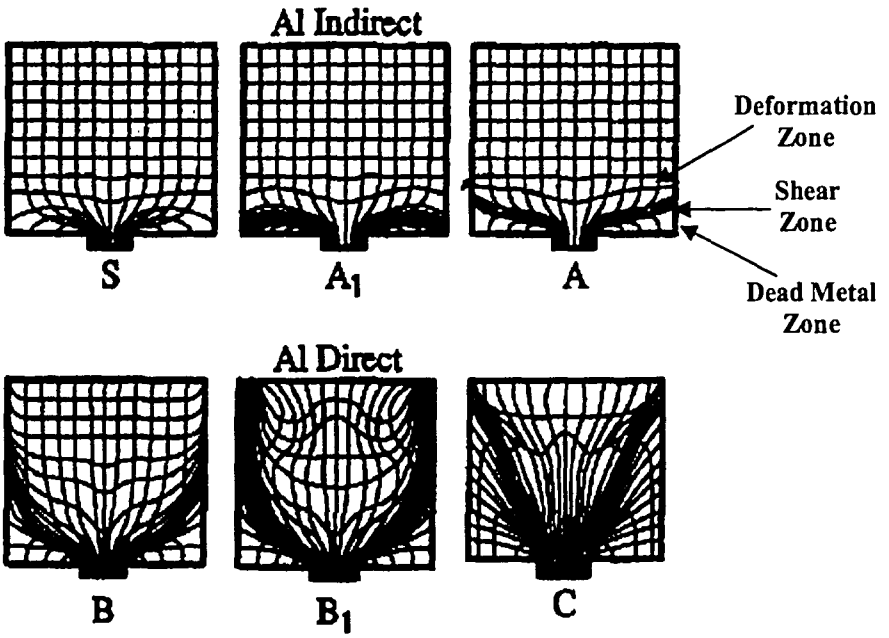

Figure 5: Modified classification system for extrusion flow including extrusion of aluminum [10].

1.2.1 Flow Types

Indirect extrusion is usually characterized by flow types S, A, and A_1, specifically for hot extrusion of aluminum. Flow pattern S is characterized by the absence of friction at the billet/container and billet/die interface during extrusion of homogeneous materials. As illustrated in Figure 5, uniform metal flow throughout the container is achieved in S-type flow. In practice, achieving S-type flow is difficult.

During the extrusion of soft alloys, A-type flow is expected to occur. Unlike S-type flow, there is significant friction at the billet/die interface in A-type flow. This friction impedes radial flow into the die possibly leading to the formation of a

dead metal zone at the die surface. A-type flow is most readily witnessed to occur in indirect extrusion [10].

Flow pattern B is characterized by friction present both at the die and container surfaces. This flow pattern is typical of most aluminum alloys under direct extrusion. As can be seen in Figure 5, B-type flow exhibits an intensive shear zone leading to a large velocity gradient at the die orifice. The intensified friction conditions lead to a larger dead metal zone located at the die corner than is witnessed in A-type flow [10].

Indirect hot extrusion of aluminum has also been found to exhibit A_1-type flow as proposed by Valberg [10]. A_1-type flow describes unlubricated indirect extrusion of aluminum and its alloys. During indirect extrusion, the billet remains stationary within the container creating friction at the billet/container interface. As the die progresses during indirect extrusion, the peripheral billet material is continuously "scraped" off the container wall and flows into the shear zone of the billet continuing to the subsurface layers of the extrudates as seen in Figure 6. Due to this scraping, a dead metal zone never forms as witnessed in A-type flow [10]. Instead, the material at the die face undergoes heavy deformation, unlike that seen in direct extrusion, and can "leak" to the surface layers of the final product. Valberg does state that some billet material can remain at the die face but will become heavily deformed as extrusion progresses [10]. Despite the claim by Valberg that a dead metal zone never forms in type A_1 flow, there is still much debate whether dead metal zone formation does actually occur during indirect extrusion. Thus, it must be

mentioned that for the purpose of this thesis, the term "dead metal zone" will be used to describe the area of metal at the die face regardless of the strain it may or may not experience.

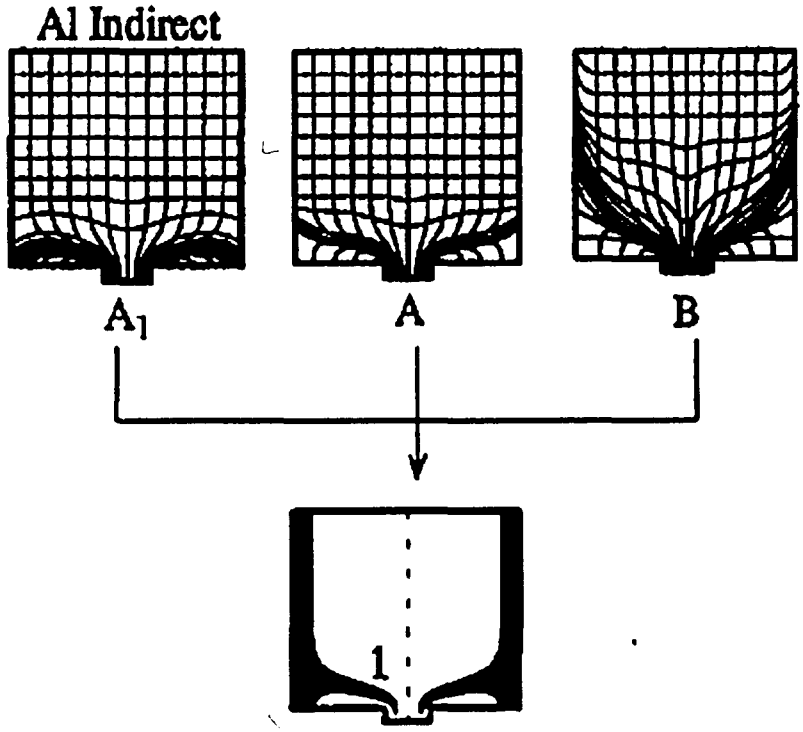

Figure 6: Surface formation for A1, A, and B type flow.

Numerous parameters affect both metal flow during extrusion and the resultant microstructure obtained. These factors include deformation temperature, material, extrusion ratio, ram speed die geometry, type of extrusion, and friction conditions. Variations in these parameters during processing can result in dramatic differences in the final extruded product [12]. These parameters must be carefully

controlled during the extrusion process to limit the occurrence of failures and ensure the appropriate final microstructure in order to obtain desired properties.

1.3 Aluminum Alloy Extrusion Metallurgy

Extrusion of aluminum alloys has become a major component of the manufacturing industry with applications ranging from aerospace, automotive, and structural components to small machined parts. The increased use of aluminum extrudates is mainly due to aluminum's high extrudability, inherent mechanical properties, corrosion resistance, and exceptional surface finish capabilities. Commonly extruded aluminum alloys include the heat-treatable 2xxx, 6xxx, and 7xxx series and non-heat treatable 1xxx, 3xxx, and 5xxx series. All commercially available alloys can be extruded with varying difficulty [6]. Table I includes nominal composition limits for commonly extruded alloys in each of these series.

Extruded products from the 2xxx and 7xxx series are widely used aerospace alloys with copper and zinc as the major alloying elements for the 2xxx and 7xxx series respectively. Characteristic of extruded 2xxx alloys is the medium to high strength, high toughness, and ductility which it exhibits. 7xxx series, like 2xxx alloys, are well known for their exceptional strength to weight ratio. 5xxx alloys contain magnesium as the primary alloy addition creating alloys of medium to high strength with good corrosion resistance.

1.3.1 6xxx Aluminum Alloy Metallurgy

Aluminum alloys in the 6xxx series are characterized by their high extrudability, resistance to corrosion, medium strength, low processing cost, weldability, and unique surface finish capabilities. 6xxx series alloys are most widely used in extruded structural applications. The most popular extruded 6xxx alloys include but are not limited to 6061 and 6063.

Magnesium and silicon are used as the major alloying additions in 6xxx series while minor alloy additions may include chromium, copper, manganese, titanium, and zinc. The research presented in this thesis was performed on two versions of 6061 alloy which will be further discussed in the section 2.1 of this thesis. A range of nominal compositions for 6061 can be seen in Table I.

Table I: Alloy chemical compostion limits (wt %) [1]

PERCENT OF ALLOYING ELEMENTS								
Alloy	**Si**	**Fe**	**Cu**	**Mn**	**Mg**	**Cr**	**Zn**	**Ti**
6061	0.4-0.8	0.7	0.14-0.40	0.15	0.8-1.2	0.04-0.35	0.25	0.15
6063	0.4	-	-	-	0.7	-	-	-
2014	0.8	-	4.4	0.8	0.50	-	-	-
2024	-	-	4.4	0.6	1.5	-	-	-
5052	-	-	-	-	2.5	.25	-	-
7075	-	-	1.6	-	2.5	.23	5.6	-

Magnesium and silicon in 6xxx alloys combine to form Mg_2Si, the principal strengthening phase in 6xxx alloys. Typically, chromium, manganese, and zirconium are added due to their proven ability to control recrystallization kinetics by pinning mobile grain boundaries thus significantly affecting the properties of 6xxx series alloys [13]. Zirconium and titanium are normally added for grain refining purposes [14]. Copper aids in solid solution strengthening of the alloy and minor additions of manganese aid in the transformation of α to spherical β-AlFeSi [15]. Iron can be found in trace amounts in most aluminum alloys as it is a naturally occurring impurity in aluminum which is retained from the ore. Normally, iron exists as α-AlFeSi intermetallics formed upon casting of 6xxx series alloys [3].

During extrusion of 6xxx alloys, it is preferred that magnesium silicide be in solid solution. This is normally achieved by homogenizing the billet prior to extrusion or extending the billet preheat time prior to deformation. Properly homogenized billets should contain uniformly distributed constituents, few insoluble iron constituents that are small and round in shape, and few visible second phase particles visible [16]. Precipitation of magnesium silicide from supersaturated solid solution occurs primarily by the clustering of Mg and Si atoms to form GP zones at temperatures normally higher than the ageing temperature. Next, coherent β" forms as needles along the <100>. β" then transforms to semi-coherent β' rods and eventually B' laths when high Si:Mg ratios are present. The final precipitates to form on the {100} are face-centered cubic Mg_2Si β platelets [17]. Morphology and distribution of Mg_2Si particles has a significant effect on both the mechanical

properties and extrudability of 6xxx series alloys. Partial precipitation of Mg_2Si upon cooling from homogenization treatments actually improves the extrudability of the material by lowering the flow stress of the alloy [6]. Care must be taken, however, to ensure the proper amount of Mg_2Si is in solution prior to extrusion to guarantee the maximum age hardening response of the alloy. An example of typical Mg_2Si β precipitates found in age hardened 6xxx series alloys can be seen in Figure 7.

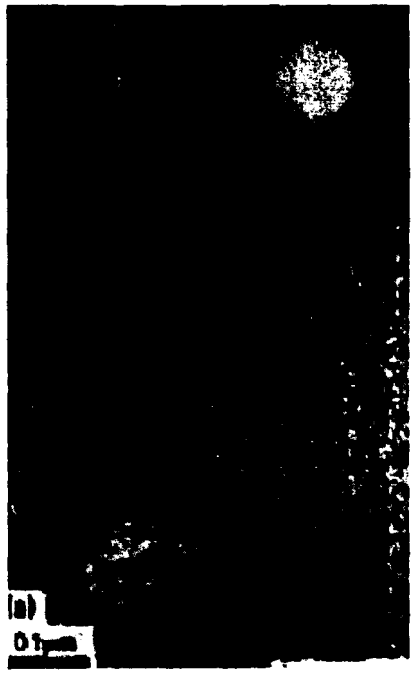

Figure 7: Example of 6xxx alloy revealing β-Mg_2Si precipitates growing in [100] direction [3].

properties and extrudability of 6xxx series alloys. Partial precipitation of Mg_2Si upon cooling from homogenization treatments actually improves the extrudability of the material by lowering the flow stress of the alloy [6]. Care must be taken, however, to ensure the proper amount of Mg_2Si is in solution prior to extrusion to guarantee the maximum age hardening response of the alloy. An example of typical Mg_2Si β precipitates found in age hardened 6xxx series alloys can be seen in Figure 7.

Figure 7: Example of 6xxx alloy revealing β-Mg_2Si precipitates growing in [100] direction [3].

1.4 Recovery and Recrystallization of Aluminum

Aluminum extrudate microstructure and properties can vary significantly depending on alloy and process parameters employed. Careful control of microstructure during extrusion is necessary to ensure the reduction of defects and homogeneity of the final product. Frequently, aluminum alloy extrudates exhibit an undesirable peripheral coarse grain (PCG) layer on the surface of an extrudate. Variations in surface structure and poor mechanical properties normally result from the presence of PCG structure in aluminum extrudates leading to increased scrap. Studies involving the reduction and eventual elimination of this phenomena are ongoing and have produced significant findings [12]. Reduction of PCG structure has been achieved by altering the following factors: increase in recrystallization inhibiting alloying elements, decrease in extrusion ration and ram speed, and control of final exit temperature [12]. An example of an extruded 6063 product with PCG can be seen in Figure 8.

Full understanding of the recovery and recrystallization processes in aluminum along with the mechanics of the extrusion process, specifically metal flow, is necessary to fully predict and control the structure evolution during hot extrusion of aluminum and its alloys.

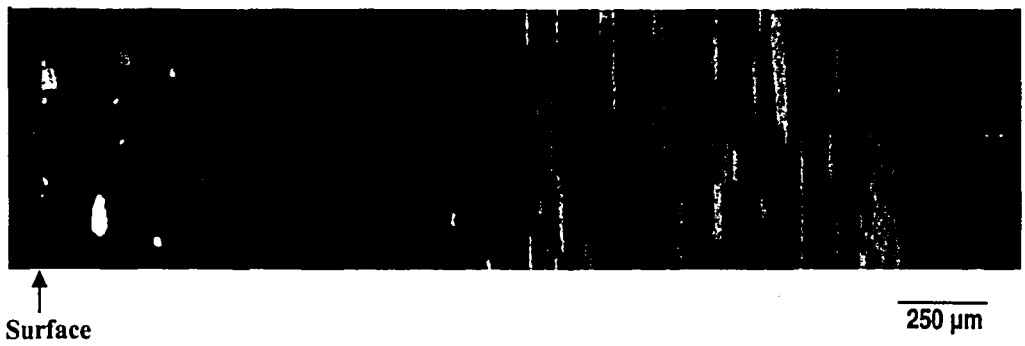

Figure 8: Aluminum 6063 alloy exhibiting common peripheral coarse grain layer at surface of extrudate.

1.4.1 Recovery of Aluminum

Recovery refers to the series of changes, primarily in the dislocation density, which occur in a deformed material either during deformation or after deformation to partially restore the properties of the deformed material to their annealed values [18]. During deformation of a material, energy is stored primarily in the form of dislocations [19]. In order to lower this stored energy, two main events occur: dislocations migration and annihilation within subgrains and subgrain growth [19].

The two most prominent recovery sub-processes are dislocation rearrangement and annihilation. These processes occur by the combination of glide, climb, and cross-slip of dislocations. Ideally, under homogeneous deformation conditions, all dislocations would annihilate. Deformation of polycrystalline materials, such as aluminum and its alloys, is usually inhomogeneous due to the processing techniques which it is subjected. Inhomogeneous deformation leads to

Figure 8: Aluminum 6063 alloy exhibiting common peripheral coarse grain layer at surface of extrudate.

1.4.1 Recovery of Aluminum

Recovery refers to the series of changes, primarily in the dislocation density, which occur in a deformed material either during deformation or after deformation to partially restore the properties of the deformed material to their annealed values [18]. During deformation of a material, energy is stored primarily in the form of dislocations [19]. In order to lower this stored energy, two main events occur: dislocations migration and annihilation within subgrains and subgrain growth [19].

The two most prominent recovery sub-processes are dislocation rearrangement and annihilation. These processes occur by the combination of glide, climb, and cross-slip of dislocations. Ideally, under homogeneous deformation conditions, all dislocations would annihilate. Deformation of polycrystalline materials, such as aluminum and its alloys, is usually inhomogeneous due to the processing techniques which it is subjected. Inhomogeneous deformation leads to

excess dislocations that can not be removed by annhiliation and thus dislocations then tend to group in subgrain boundaries [20]. The main stages of recovery in hot deformation can be seen schematically in Figure 9. A subgrain boundary is defined by a low angle grain boundary. Mean misorientations of subgrain boundaries have been calculated and reported [21].

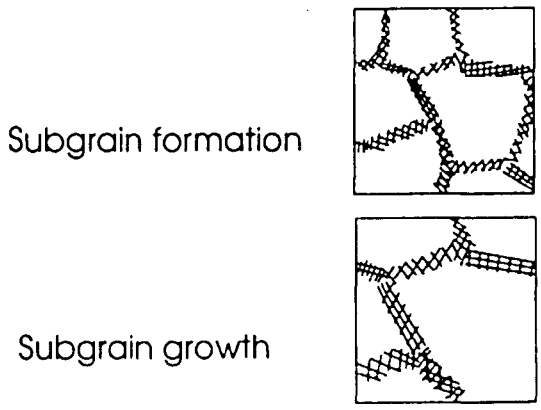

Figure 9: Stages during the recovery of a plastically deformed material[18]

There are many factors which affect the degree and rate of dynamic recovery in deformed materials. These factors include stacking fault energy, strain, and deformation temperature. The stacking fault energy, γ_{SFE}, is a crucial parameter in determining the rate at which dislocations will undergo climb and cross-slip. Aluminum has a high stacking fault energy of approximately 200 mJ/m^2 [4]. Dislocation climb in materials such as aluminum with high stacking fault energies occurs easily, thus dynamic recovery occurs readily.

1.4.2 Recrystallization of Aluminum

Recrystallization is defined by the formation of a new grain structure by the migration of high angle grain boundaries in a deformed material. Recrystallization, like recovery, can occur either during or after deformation known as dynamic or static recrystallization. Dynamic recrystallization can be broken down into two categories: continuous dynamic recrystallization (cDRX) and discontinuous dynamic recrystallization (dDRX). These subsets of dynamic recrystallization can be distinguished between those with nucleation events and those without. dDRX operates by nucleation and growth whereas cDRX by the transformation of low to high angle boundaries by dislocation accumulation and annihilation [22]. Static recrystallization refers to the post-deformation annealing phenomenon occurring in deformed materials such as aluminum alloys.

During extrusion of aluminum, it is difficult to distinguish between which recrystallization events are taking place, those occurring statically or those occurring dynamically. This difficulty is due to the time lapse between the completion of extrusion and quenching. The following sections will provide descriptions of the various recrystallization events described above.

1.4.2.1 Dynamic Recrystallization

1.4.2.1.1 Discontinuous Recrystallization

As previously stated, dDRX occurs via a nucleation and growth process. Typically, dDRX occurs in low stacking fault energy metals; however, it has been found to occur in high purity aluminum and aluminum alloys containing large particles. Nuclei of dDRX must have highly misoriented boundaries to allow for easy mobility. Nucleation sites may include pre-existing high angle grain boundaries, highly misoriented deformation zones around large particles, or highly misoriented regions within shear bands [19]. The condition for nucleation of a dynamically recrystallized grain can be described by the following relationship:

$$\rho_m^3/\dot{\varepsilon} > 2\gamma_b/KMLGb^5$$

where;

ρ_m = dislocation density
$\dot{\varepsilon}$ = strain rate
γ_b = grain boundary energy
K = constant
L = mean slip distance of dislocations
M = boundary mobility
G = shear modulus
b = Burgers vector [18].

The left hand side of the equation, $\rho_m^3/\dot{\varepsilon}$, must reach a critical value for dynamic recrystallization to nucleate. The right hand side of the equation is assumed to remain constant for deformation at a given temperature. As stated before, aluminum and its alloys recover easily due to its high stacking fault energy thus the

dislocation density within such materials never reaches the critical value required for dynamic recrystallization.

1.4.2.1.2 Continuous Recrystallization

cDRX operates by the accumulation of dislocations in low angle subgrain boundaries. These low angle boundaries transform into movable high angle boundaries by the continuous accumulation of dislocations at the boundary. This phenomena has also been termed "extended recovery" as recovery processes contribute to the development of high angle boundaries [19].

1.4.2.2 Geometric Recrystallization

The phenomena known as geometric dynamic recrystallization (gDRX) has been confirmed to occur in Al-Mg alloys and also is suspected to occur in alloys that experience dynamic recovery [19]. Geometric dynamic recrystallization is defined by the formation of a new grain by change in the original grain geometry during deformation to high strain [20]. In high stacking fault energy materials such as aluminum alloys, dynamic recovery occurs by dislocation climb, glide, and cross-slip resulting in the formation of low angle boundaries. During deformation, grain boundaries become serrated as a result of dynamic recovery leading to the interaction of subgrain boundaries with existing high angle grain boundaries. The serrations that result from such interactions can be seen schematically in Figure 10.

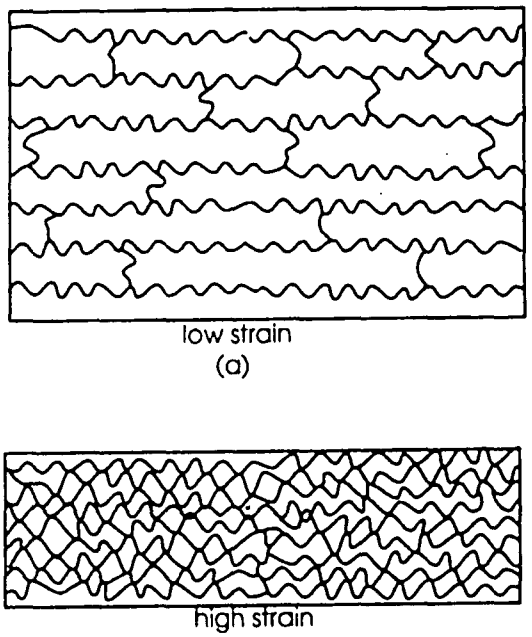

Figure 10: Schematic of the formation of gDRX at (a) low and (b) high strains [18].

After larger strains, serrated grains elongate to a thickness of approximately twice the subgrain size [22]. As grains thin, impingement of pre-existing high angle grain boundaries with subgrain boundaries occurs. These impingements cause new high angle grains containing little substructure to pinch off from pre-existing high angle grain boundaries. Geometrically recrystallized microstructures usually consist of small equiaxed grains approximately two to three times the subgrain size primarily of high angle boundaries [19, 20, 22-25]. Figure 11 reveals a geometrically recrystallized structure.

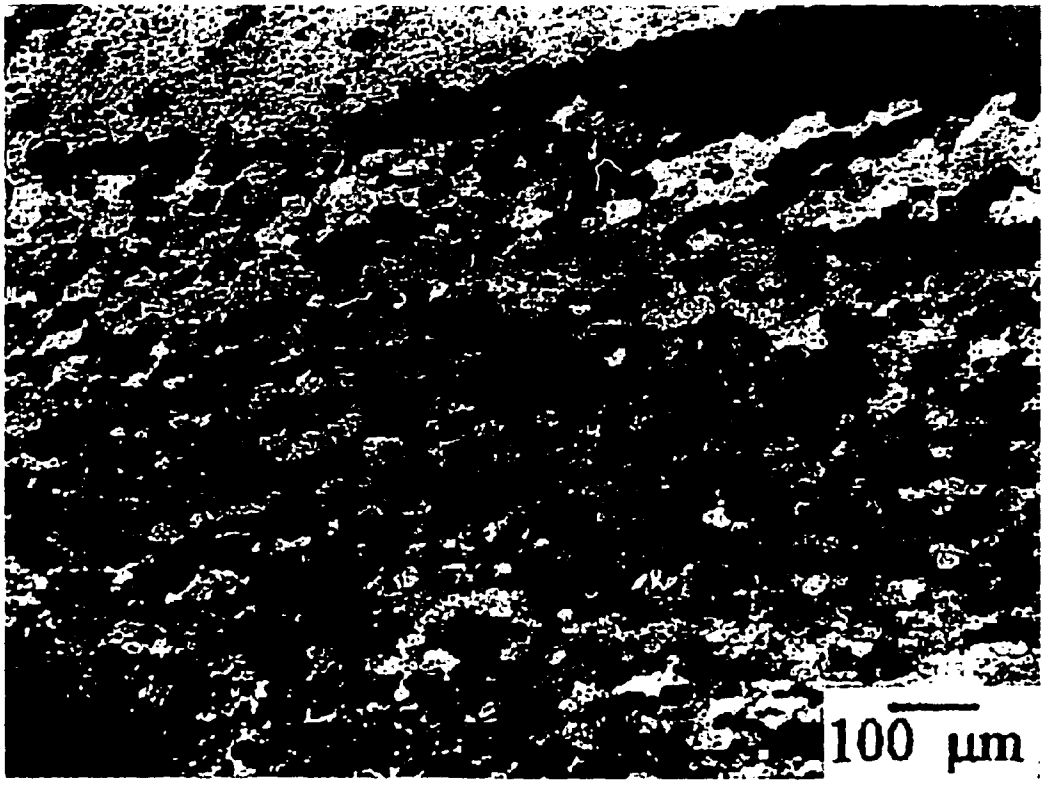

Figure 11: Microstructure of Al (<99.99) deformed to $\varepsilon = 40$ at 400°C and .2 s^{-1} revealing geometrically recrystallized grains [26].

1.4.2.3 Static Recrystallization

Static Recrystallization (SRX) can occur in deformed materials such as aluminum alloys when they receive some post-deformation thermal treatment. Depending on the stored energy present within the deformed material, static recrystallization can occur rapidly. Figure 12 shows the effect of deformation temperature and strain rate described by the Zener-Hollomon parameter on the kinetics of static recrystallization. This figure strongly demonstrates the effect of processing parameters on recrystallization kinetics.

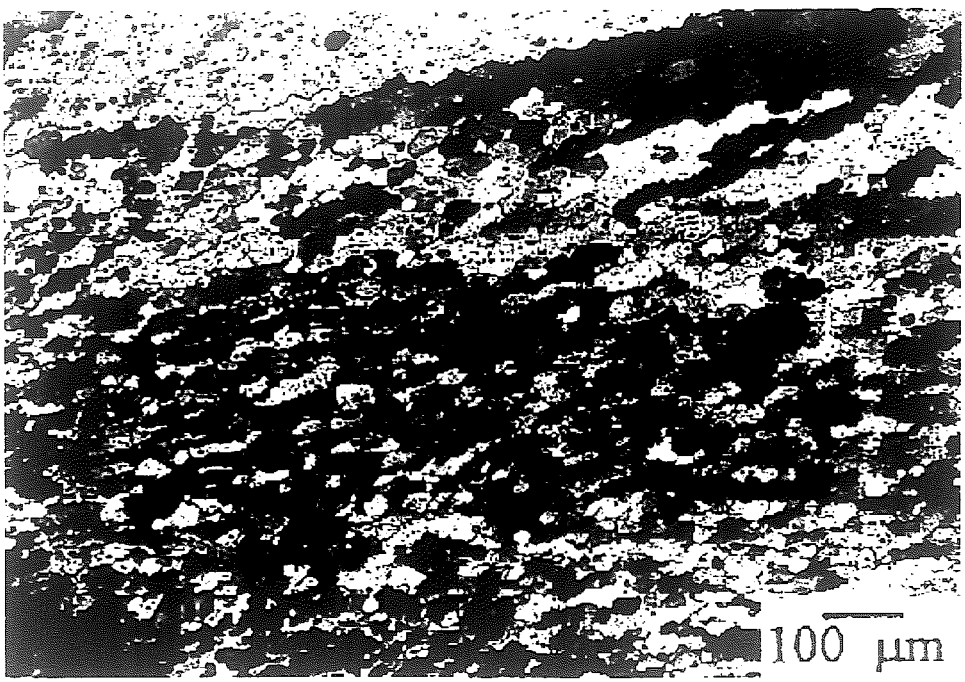

Figure 11: Microstructure of Al (<99.99) deformed to $\varepsilon = 40$ at 400°C and .2 s^{-1} revealing geometrically recrystallized grains [26].

1.4.2.3 Static Recrystallization

Static Recrystallization (SRX) can occur in deformed materials such as aluminum alloys when they receive some post-deformation thermal treatment. Depending on the stored energy present within the deformed material, static recrystallization can occur rapidly. Figure 12 shows the effect of deformation temperature and strain rate described by the Zener-Hollomon parameter on the kinetics of static recrystallization. This figure strongly demonstrates the effect of processing parameters on recrystallization kinetics.

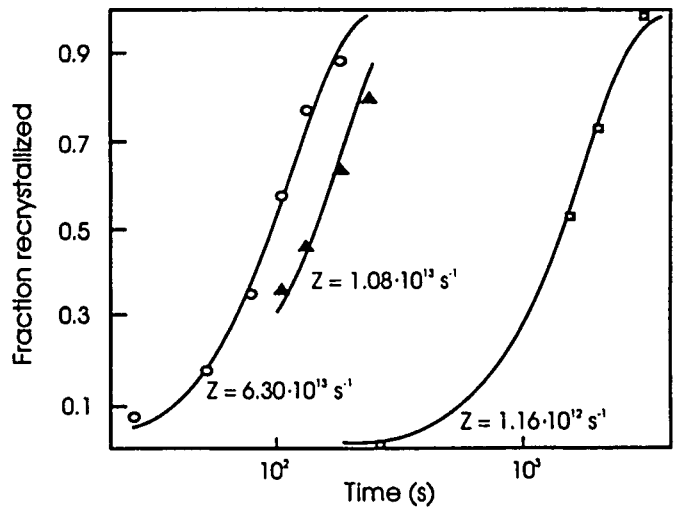

Figure 12: Effect of Z parameter (strain rate and deformation temperature) on recrystallization kinetics [7].

2.0 EXPERIMENTAL PROCEDURE

2.1 Billet Material

The testing matrix for this research was comprised of two 6061 alloys, identified as high chromium and low chromium. The high chromium alloy contained a 2:1 chromium to manganese ratio; whereas, the low chromium alloy contained a 1:1 chromium to manganese ratio. Small scale billets were machined from the mid-radius of homogenized, Direct Chill (DC)-cast industrial billets to a diameter of 30.5 mm and length of 50.8 mm. Normally, structural inhomogeneities are more pronounced at the surface of a DC-cast billets due to reheating of surface layers during casting. Therefore, obtaining samples from the mid-radius ensured a more homogenous cast structure leading to few defects in the final extrudate.

Homogenization of industrial sized billets was performed at Alcoa Engineered Products, in Cressona, PA. A proprietary industrial homogenization treatment was performed on both the high and low chromium billets.

2.2 Small-Scale Indirect Extrusions

Small-scale indirect extrusions were performed on a servo-hydraulic deformation simulator at Alcoa's Technical Center in Alcoa Center, PA. Table II displays the testing matrix of the experiments performed. Varying extrusion ratios and ram speeds were used at 400°C to evaluate the effect of strain and strain rate on metal flow during extrusion and final extrudate microstructure. All tests were performed at 400°C. Testing parameters were chosen based on previously reported

results of reduced PCG depth [12]. Tests performed were interrupted at 25, 50, and 75% completion to evaluate the evolution of structure throughout the extrusion process. Interrupted extrusions performed on the low chromium alloy were only performed at one testing condition as described by the matrix below as a standard for comparison.

Small-scale billets and tooling were preheated to 400°C prior to extrusion. A hold time of 30 seconds at 400°C was applied prior to the start of extrusion to ensure adequate heating of the billet and surrounding tooling. Indirect extrusions were completed when the billet was extruded to the desired length as described by the testing matrix in Table II. Actual discard lengths varied slightly from the proposed lengths and will be discussed in the next section. K-type thermocouples located on the die face, the extrusion ram, and in three positions (lower, center, and upper) on the container recorded relevant temperatures during extrusion. Extrudates were immediately quenched with a water mist at the die exit. Remaining discard lengths were also quenched with a water spray approximately 30 seconds after completion of the extrusion process. At the onset of quenching, butt samples were quenched to room temperature within 2-3 seconds as determined by the die face thermocouple. Since this thermocouple collects the temperature of the steel die, the quench rate for the partially extruded billet is expected to be faster than the recorded data.

Table II: Testing matrix for small-scale indirect extrusions performed on deformation simulator at Alcoa's Technical Center.

Sample	Alloy	Ram Speed (mm/s)	Extrusion Ratio	Deformation Temperature (°C)	% Completion
885	High Chromium	2.6	20	400	25%
880	High Chromium	2.6	20	400	50%
883	High Chromium	2.6	20	400	75%
891	High Chromium	1.3	20	400	25%
889	High Chromium	1.3	20	400	50%
887	High Chromium	1.3	20	400	75%
884	High Chromium	2.6	40	400	25%
879	High Chromium	2.6	40	400	50%
881	High Chromium	2.6	40	400	75%
890	High Chromium	1.3	40	400	25%
893	High Chromium	1.3	40	400	50%
886	High Chromium	1.3	40	400	75%
894	Low Chromium	1.3	20	400	75%
895	Low Chromium	1.3	20	400	50%
896	Low Chromium	1.3	20	400	25%

2.3 Light Optical Microscopy

Partially extruded billets and extrudates taken from the steady state region from each testing condition were sectioned and ground to mid-diameter. Samples were metallographically prepared to investigate the evolution of metal flow and development of billet and extrudate microstructure during extrusion. Samples were polished using 1 μm Al_2O_3 and 0.05 μm colloidal silica (SiO_2). Samples were electrolytically etched at 30 V for 5 minutes using a modified Barker's reagent comprised of 2.5% HBF_4, 25% of 30% H_2O_2, and distilled water. Polarized Light Optical Microscopy (PLOM) was used to analyze both partially extruded billet and final extrudate microstructures for all testing conditions.

2.4 Billet Evolution Quantification

The main objective of this thesis was to characterize metal flow evolution within aluminum 6061 billets during indirect extrusion. In order to completely characterize billet evolution, specifically the development of certain deformation zones present during extrusion, the area of dead metal zones and the transition from the dead metal zone to the shear zone needed to be investigated. This can be performed through the assessment of the microstructural transition from fine equiaxed grains present in the dead metal region to highly deformed grains within the intensive shear zone. Accurately defining an abrupt interface to this area proved to

be difficult as the structure within the transition zone is usually quite diffuse with the structure constantly varying from fine equiaxed grains to elongated bands.

2.4.1 Experimental Techniques for Billet Characterization

Characterization of billet evolution during indirect extrusion required the investigation of numerous analytical methods. Initially, LOM was utilized to determine the depth of the dead metal zone for all samples. Depths were obtained at two separate times at the same position on each partially extruded sample. Obtaining depths using this method proved subjective and not accurate which led to the utilization of Electron Backscatter Diffraction (EBSD), which will be discussed in greater detail in the following section, for improved resolution.

Grain shape aspect ratios were obtained from orientation maps produced using EBSD. Aspect ratios for all grains contained within one EBSD scan were imported into Mathcad graphing software. It was expected that a clear transition from the dead metal zone to the shear zone would be observed by plotting aspect ratio versus distance from the die face. Results obtained from this method did not provide an accurate definition of the transition from the dead metal zone to the shear zone.

Failure of the aforementioned techniques helped to provide the most effective approach for characterizing billet evolution as will be discussed in the following section.

2.4.2 Electron Backscatter Diffraction (EBSD)

The Electron Backscatter Diffraction (EBSD) technique was performed using a TexSEM Laboratories (TSL) system interfaced with a Philips XL 30 ESEM to further analyze dead zone geometry, metal flow, and structure evolution within partially extruded billets. EBSD is advantageous over LOM in that useful microtextural and microstructural information can be obtained simultaneously.

Samples chosen for EBSD analysis included 885, 880, and 883, as described in Table II, representing 25, 50, and 75% of billet deformation at a ram speed of 2.6 mm/s with an extrusion ratio of 20. Samples for EBSD analysis were re-polished using 1 μm Al_2O_3, 0.05 μm colloidal silica, and, finally, were chemically polished. The chemical polish solution comprised of HNO_3, HPO, H_2SO_4 was applied to each sample to remove any surface deformation resulting from polishing and any oxide on the surface.

Scans positioned across the die face were performed on each sample to accurately characterize dead metal zone geometry. Locations of each scan changed from sample to sample as actual dead metal zone geometries varied as displayed from light optical microscopy results. Actual scan positions on sample surfaces were determined from deposits remaining on sample surfaces after scans were complete. SEM and EBSD images of these scan deposits can be seen in Figure 13 (a-b). Depths of each scan also varied depending on the position of the scan in reference to the approximate depth of the dead metal zone as dictated by previous LOM results.

Actual scan positions for each sample can be seen in Tables III-V. Scan position measurements were taken from the top left corner of each scan as described schematically in Figure 14. Plots of the scan positions for samples 880, 883, and 885 can be seen in Figures 15-17.

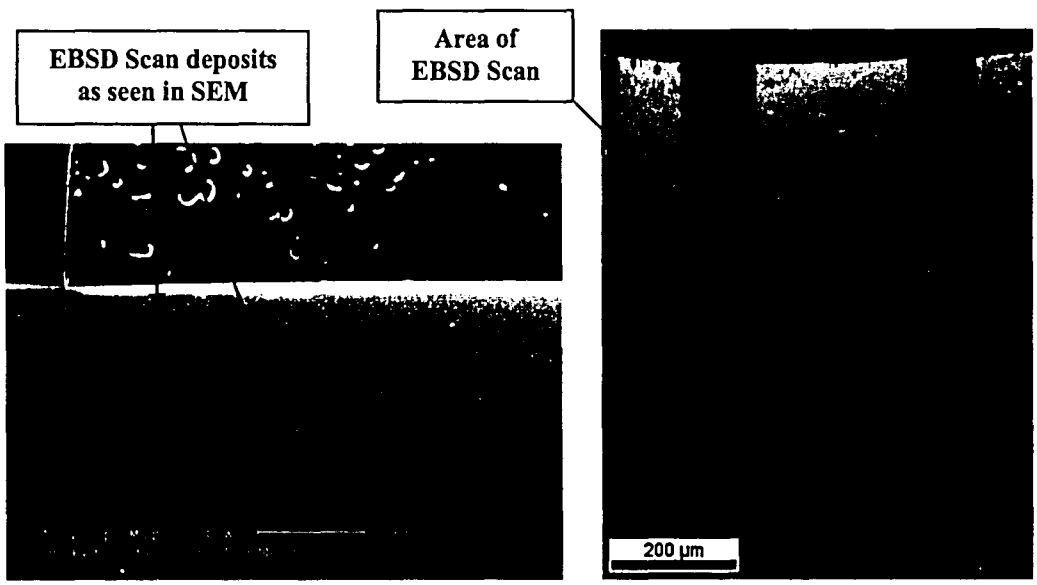

Figure 13: Images of EBSD scans from sample 883 taken with (a) SEM and (b) OIM software performed on partially extruded sample.

Actual scan positions for each sample can be seen in Tables III-V. Scan position measurements were taken from the top left corner of each scan as described schematically in Figure 14. Plots of the scan positions for samples 880, 883, and 885 can be seen in Figures 15-17.

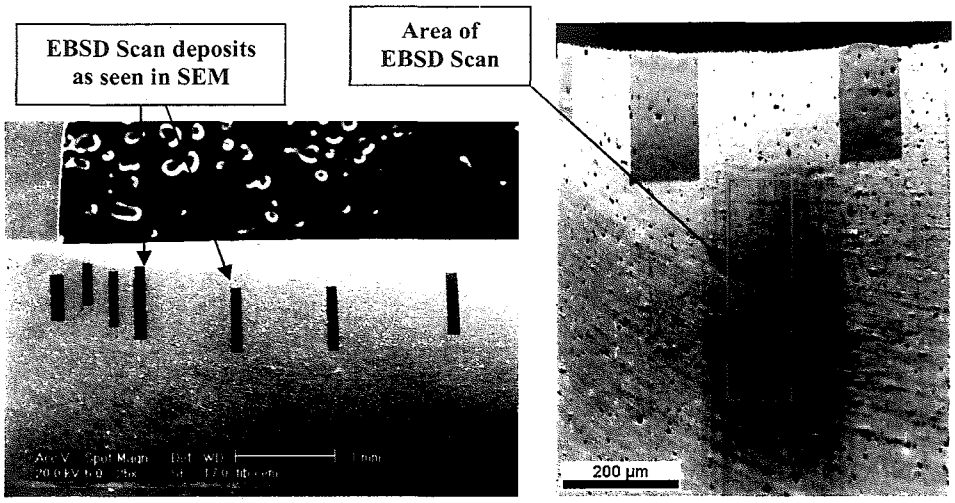

Figure 13: Images of EBSD scans from sample 883 taken with (a) SEM and (b) OIM software performed on partially extruded sample.

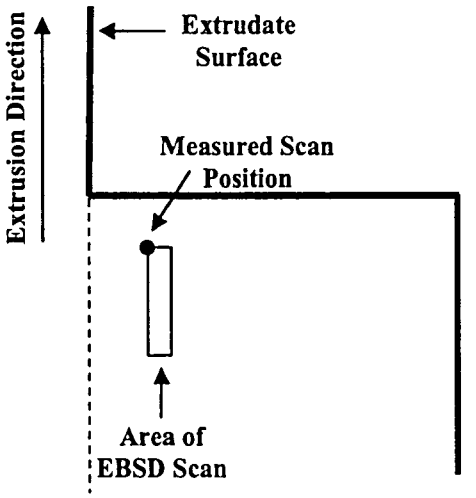

Figure 14: Schematic revealing location of scan position measurements. Position measurements were taken from the top left corner of each scan.

Table III: Scan positions for sample 883.

SCAN POSITIONS SAMPLE #883		
SCAN #	Position from extrudate surface (μm)	Position from Die face (μm)
1	433.89	187.85
2	686	156.86
3	1627	392.16
4	2549	333
5	3706	254.9
6	4765	333
7	6940	352.9
8	8465	316

Table IV: Scan positions for sample 880.

SCAN POSITIONS SAMPLE #880		
SCAN #	Position from extrudate surface (μm)	Position from Die face (μm)
1	354.9	225.2
2	1365	155.56
3	1819	169.84
4	2326	390.48
5	3354	338.09
6	4053	403.17
7	7202	42.86

Table V: Scan positions for sample 885.

SCAN POSITIONS SAMPLE #885		
SCAN #	Position from extrudate surface (μm)	Position from Die face (μm)
1	95.23	66.66
2	644.4	23.8
3	1415.83	266.6
4	1777.73	123.8
5	3311.91	115.87
6	4982.85	123.89
7	6824.7	0
8	7756.32	0

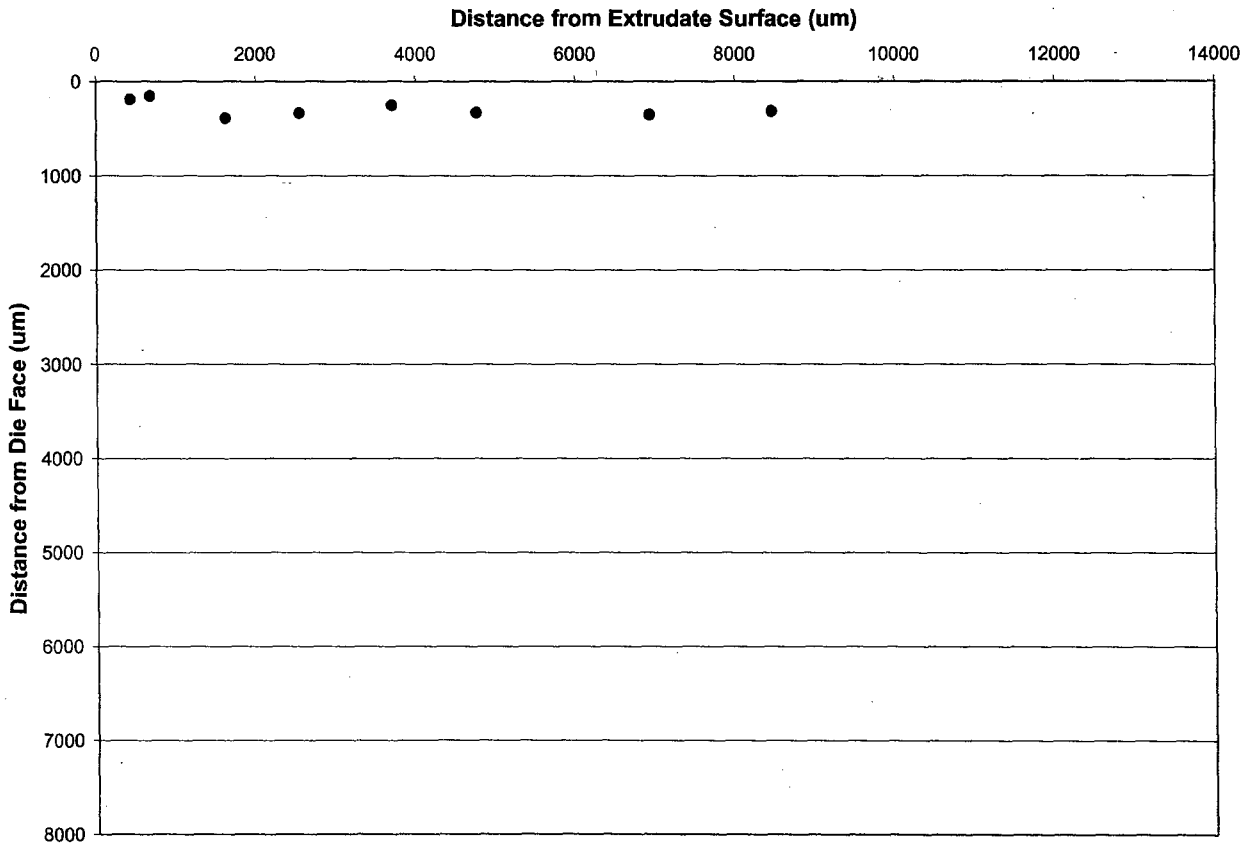

Figure 15: Plot of EBSD scan positions for sample 883.

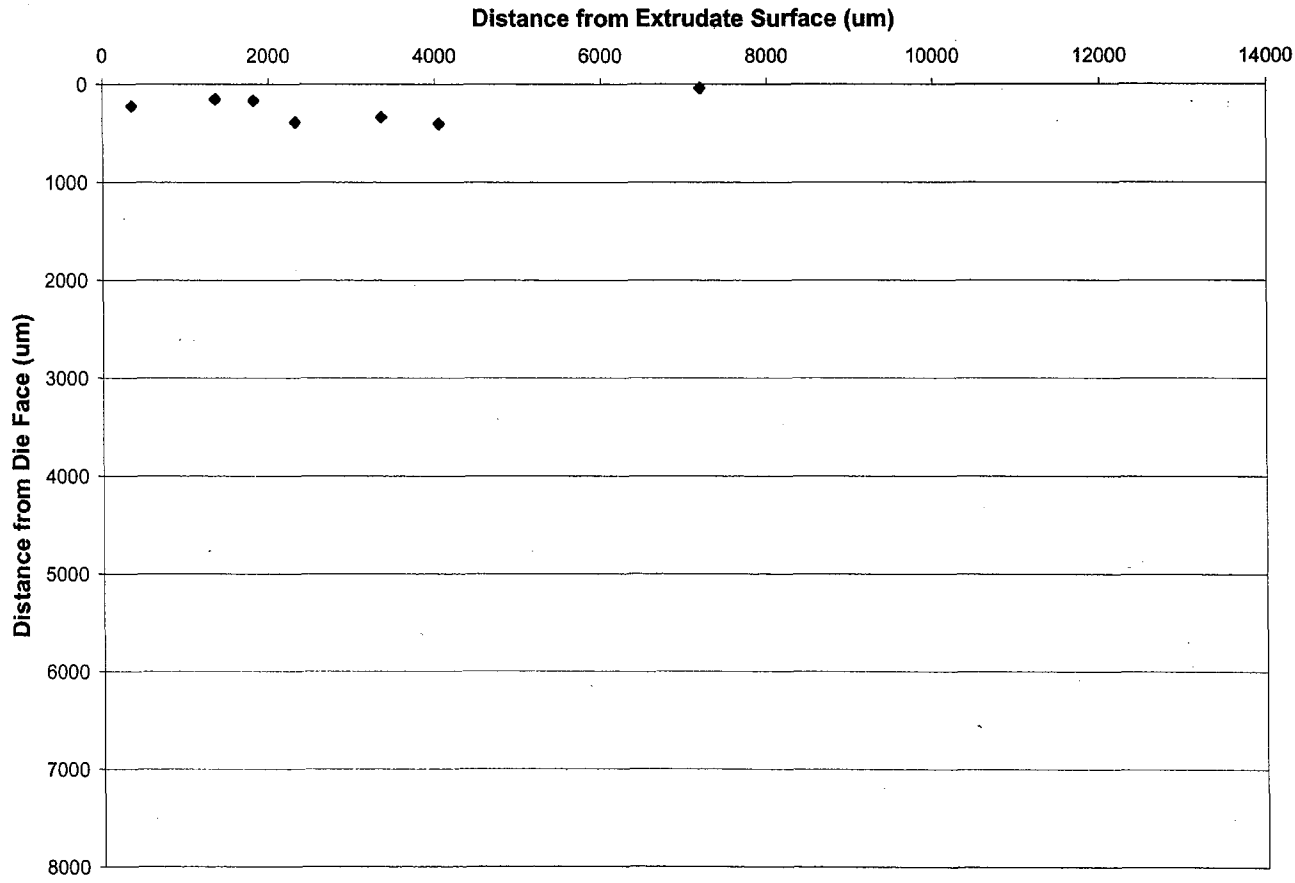

Figure 16: Plot of EBSD scan positions for sample 880.

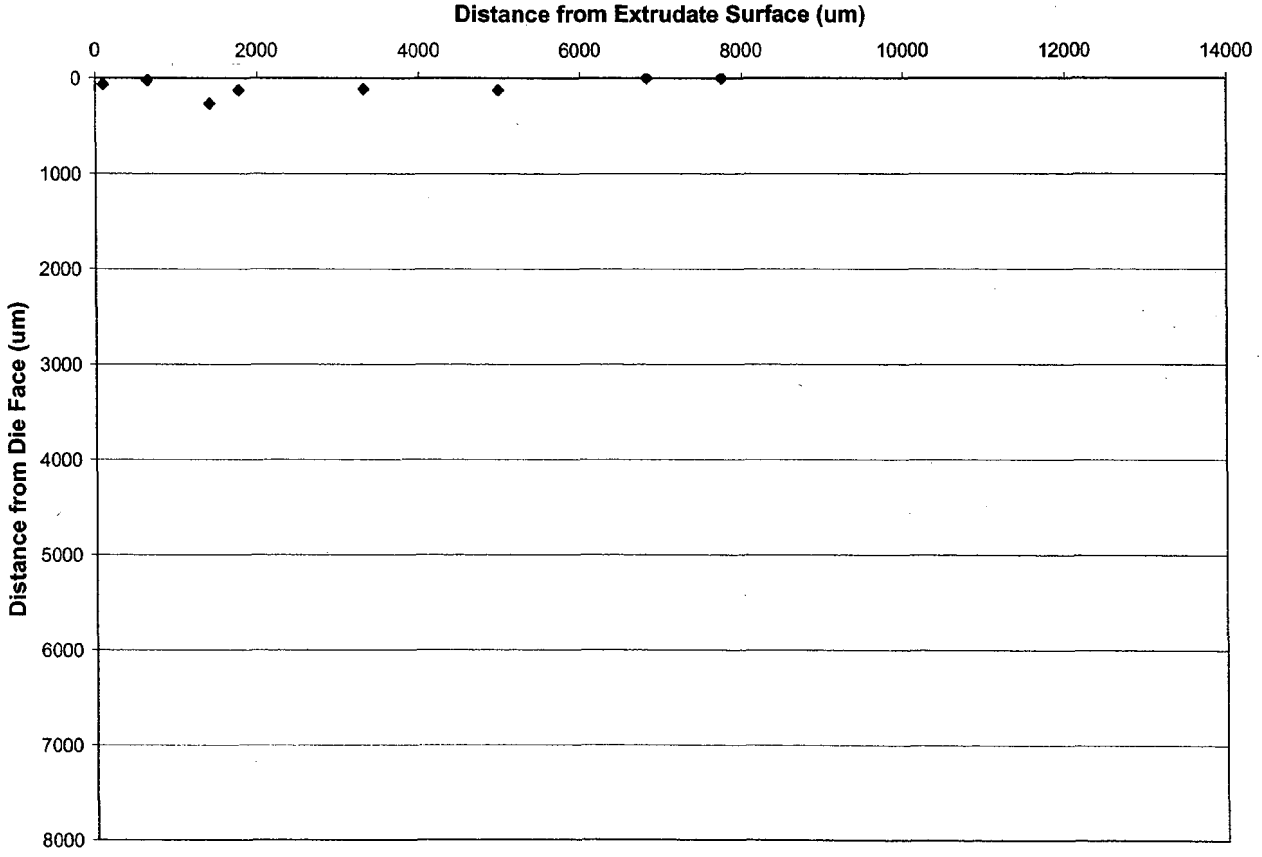

Figure 17: Plot of EBSD scan positions for sample 885.

2.4.3 Dead Metal Zone Geometry Calculations

In quantifying both dead metal zone geometry and area using grain size maps, it is crucial to define the structural features witnessed in order to make measurements less subjective. In order to provide consistency, the end of "continuous" dead metal zone was determined in the location where long deformed grains were first witnessed to form. This transition in microstructure was difficult to resolve using orientation maps; thus, grain size maps were generated using OIM software. With a grain size map, each grain is assigned a color based on the grain diameter as determined by OIM analysis software. The assigned colors ranged from blue to red as grain diameter increased. The grain size maps generated allowed for easy visualization of the microstructural gradients present within the partially extruded billets. For each map, the grain tolerance angle was set to 15° therefore ensuring no subgrains of low misorientation (<15°) were included in generating both the grain size maps and orientation maps.

As previously stated, assigning a sharp interface to the transition from dead metal to deformed metal is difficult. In order to accurately represent this diffuse region, three measurements were taken per grain size map. The first measurement was taken at the end of the "continuous" dead metal zone, as previously described. The second measurement was taken in an area between "continuous" dead metal zones and "continuous" deformed grains representing an average depth of the transition zone. The third and final measurement was taken where long deformed

grains continuously neighbored each other representing a complete transition into the shear zone. In some cases, as will be discussed later, maps generated did present a sharp delineation between the dead metal zone and shear zone. In such cases, one measurement was taken at this interface. Measurements were then imported into Mathcad and Excel software to obtain dead metal zone geometry projections and dead metal zone area measurements for 25, 50, and 75% extruded billets. Figure 18 provides an example of both an orientation map and grain size map. Within the grain size map, a schematic of the three measurements defining the transition zone described above are shown.

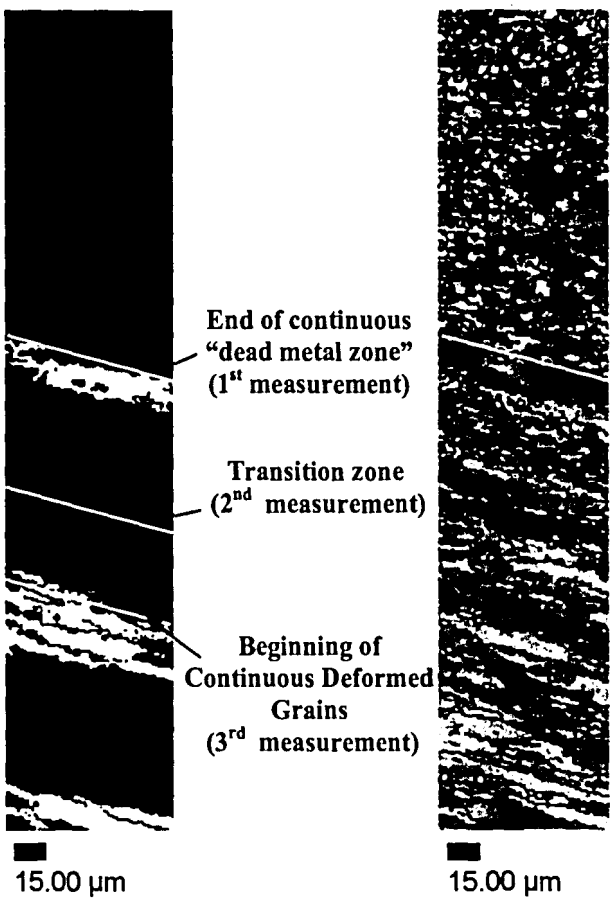

Figure 18: Definition of transition from dead metal zone to beginning of deformed shear region for (a) grain size map and (b) orientation map taken near die exit of sample 883.

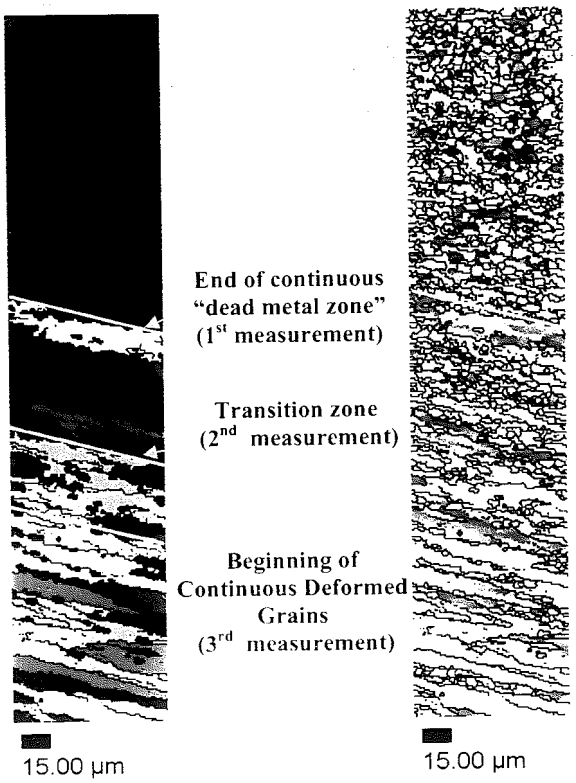

Figure 18: Definition of transition from dead metal zone to beginning of deformed shear region for (a) grain size map and (b) orientation map taken near die exit of sample 883.

3.0 RESULTS

3.1 Small-Scale Indirect Extrusion Results

During small-scale indirect extrusion tests, load, ram stroke and speed, as well as, temperature were recorded. Presented below in Figure 19-21 are breakthrough load versus ram stroke data from small-scale extrusion experiments for each series of test parameters. Results seen here are typical of an indirect extrusion process including upsetting, breakthrough, and steady state region. A large variation in extrusion breakthrough load can be seen in Figure 20 (a-b) for extrusion ratio of 20 and ram speeds of both 1.3 and 2.6 mm/sec. It is expected that extrusion loads for each series of testing parameters remain similar throughout extrusion. Large variations in breakthrough pressures may alter final microstructures seen for the same extrusion test parameters. Figures 19-20 reveal an increase in breakthrough load as ram speed and extrusion ratio increase.

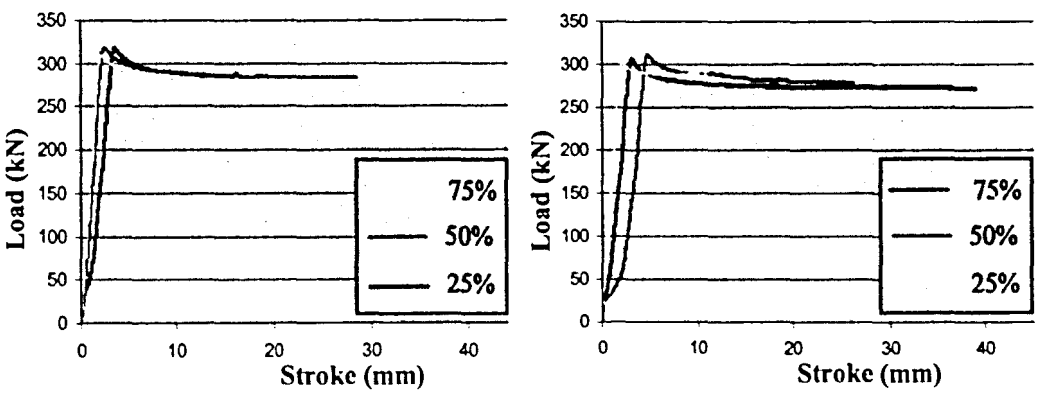

Figure 19: Load versus stroke data for testing conditions (a) R=40 and ram speed of 2.6mm/s and (b) R=40 and ram speed of 1.3 mm/s.

3.0 RESULTS

3.1 Small-Scale Indirect Extrusion Results

During small-scale indirect extrusion tests, load, ram stroke and speed, as well as, temperature were recorded. Presented below in Figure 19-21 are breakthrough load versus ram stroke data from small-scale extrusion experiments for each series of test parameters. Results seen here are typical of an indirect extrusion process including upsetting, breakthrough, and steady state region. A large variation in extrusion breakthrough load can be seen in Figure 20 (a-b) for extrusion ratio of 20 and ram speeds of both 1.3 and 2.6 mm/sec. It is expected that extrusion loads for each series of testing parameters remain similar throughout extrusion. Large variations in breakthrough pressures may alter final microstructures seen for the same extrusion test parameters. Figures 19-20 reveal an increase in breakthrough load as ram speed and extrusion ratio increase.

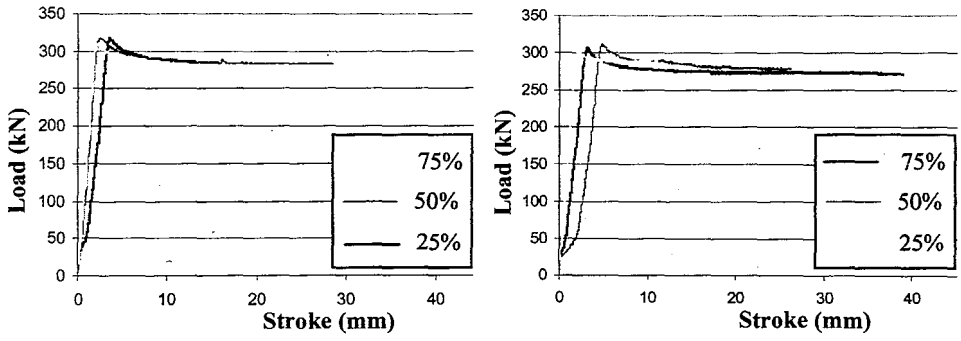

Figure 19: Load versus stroke data for testing conditions (a) R=40 and ram speed of 2.6mm/s and (b) R=40 and ram speed of 1.3 mm/s.

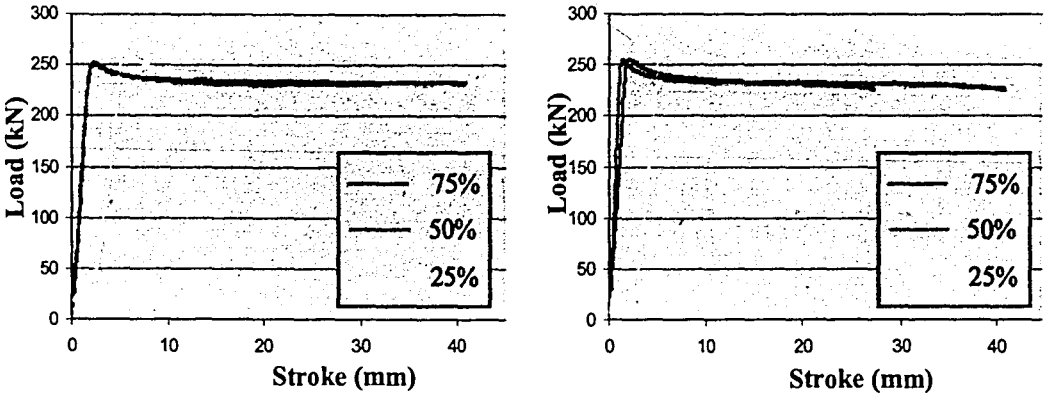

Figure 20: Load versus stroke data for testing conditions (a) R=20 and ram speed of 1.3 mm/s and (b) R=20 and ram speed of 2.6 mm/s.

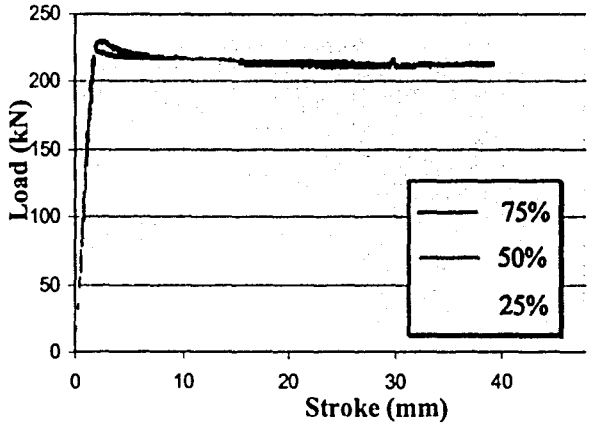

Figure 21: Load versus stroke data for low chromium samples and testing conditions of R=20 and ram speed of 1.3 mm/s.

Ram velocity for each testing condition remained constant during the test at its programmed value of 1.3 mm/s or 2.6 mm/s. A typical temperature profile at the die face during indirect extrusion to 75% completion can be seen in Figure 22. Maximum deformation temperatures recorded at the die face ranged between 420-430°C.

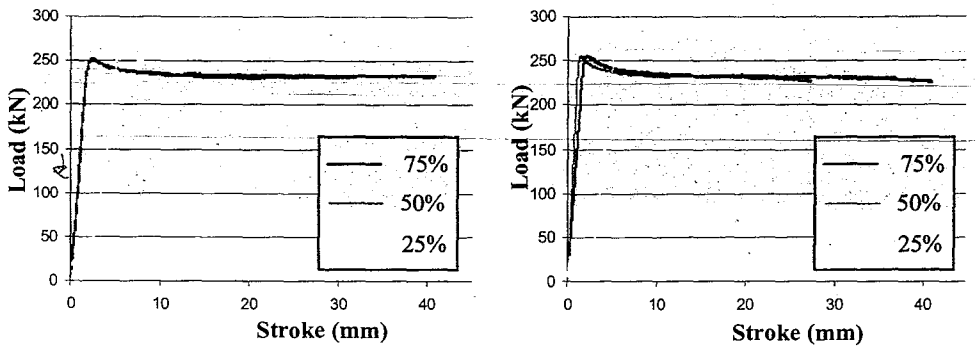

Figure 20: Load versus stroke data for testing conditions (a) R=20 and ram speed of 1.3 mm/s and (b) R=20 and ram speed of 2.6 mm/s.

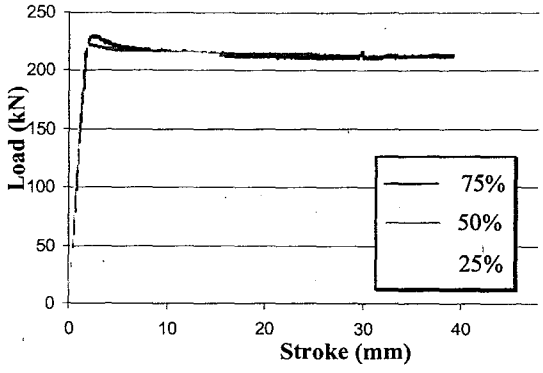

Figure 21: Load versus stroke data for low chromium samples and testing conditions of R=20 and ram speed of 1.3 mm/s.

Ram velocity for each testing condition remained constant during the test at its programmed value of 1.3 mm/s or 2.6 mm/s. A typical temperature profile at the die face during indirect extrusion to 75% completion can be seen in Figure 22. Maximum deformation temperatures recorded at the die face ranged between 420-430°C.

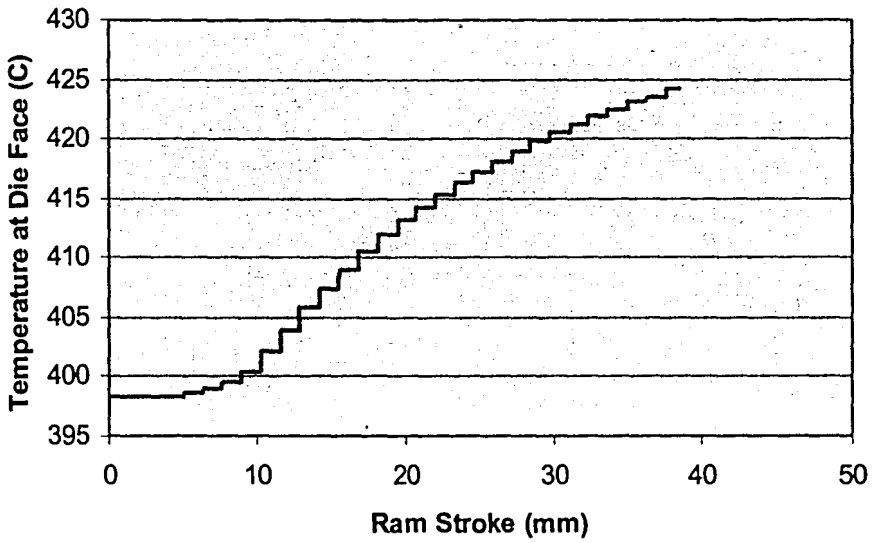

Figure 22: Plot revealing typical temperature profile at die face during indirect extrusion as a function of ram stroke.

Proper investigation of dead metal zone evolution extrusion requires knowledge of the actual percentage of the billet extruded. Extrusion tests were programmed to terminate when 25, 50, and 75% of the billet was extruded. However, the actual extruded lengths varied significantly from the programmed length as seen in Table III. The percentage of error for extrusion runs, as seen in Table VI, ranged from 1.8% to 38%.

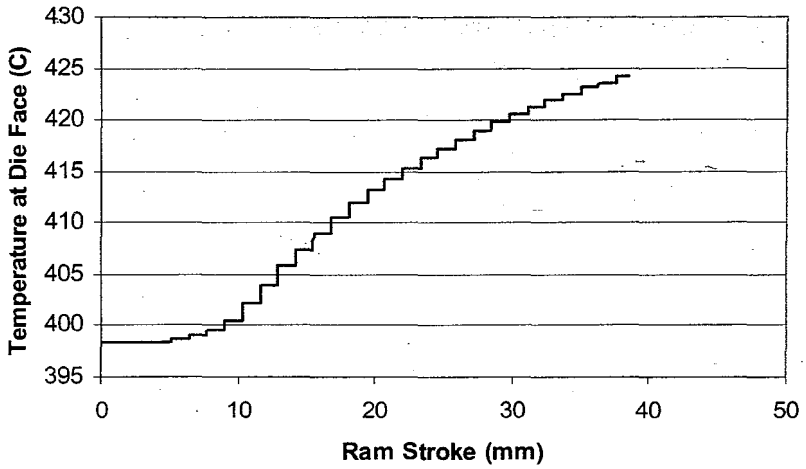

Figure 22: Plot revealing typical temperature profile at die face during indirect extrusion as a function of ram stroke.

Proper investigation of dead metal zone evolution extrusion requires knowledge of the actual percentage of the billet extruded. Extrusion tests were programmed to terminate when 25, 50, and 75% of the billet was extruded. However, the actual extruded lengths varied significantly from the programmed length as seen in Table III. The percentage of error for extrusion runs, as seen in Table VI, ranged from 1.8% to 38%.

Table VI: Actual percentage billet partially extruded.

Sample	Actual billet length (mm)	Average billet Length (mm)	%Error	Actual percentage extruded
885	38.1	38.9	2.1	23.43
880	25.4	19.90	21.67	60.83
883	12.7	7.87	38.07	84.50
891	38.1	38.8	1.84	23.62
889	25.4	22.6	11.014	55.51
887	12.7	8.82	30.554	82.64
884	38.1	36.9	3.15	27.36
879	25.4	20.8	18.084	59.04
881	12.7	8.56	32.55	83.14
890	38.1	33.94	10.93	33.2
893	25.4	25.94	2.14	48.93
886	12.7	11.17	12.02	78.01
894	12.7	10.01	21.18	80.3
895	25.4	21.13	16.81	58.41
896	38.1	32.17	15.56	36.67

3.2 Small-Scale Indirect Extrusion Microstructures

3.2.1 Partially Extruded Billet Microstructures

6061 partially extruded billet microstructures for the high and low chromium alloys taken from the die corner to the die orifice can be seen in Figure 23-36. Metal flow patterns present in these figures strongly suggest A_1-type flow as proposed by Valberg described earlier. Characteristic of this flow type is the concavity of the intensive shear zones which can be seen in Figures 23-36.

Within these zones, a distinct variation in structure, specifically dead metal and shear zone geometry, exists as extrusion progresses from 25 to 75% completion. Highly deformed large grains within the shear zone were witnessed to form in all 25% extruded samples whereas fine banded grains are seen within the concave shear zone of 50 and 75% extruded samples. Increased magnification reveals serrated grain boundaries and fragmentation of grains primarily along the dead metal/shear zone interface. Evidence of grain fragmentation can be seen in Figure 37. LOM also reveals that deformed grains visible within the shear zone of 25% samples develop into the "dead" metal zone as extrusion progresses through 75% completion. This progression along with the results of dead zone geometry predictions will be discussed later with presented results of EBSD analysis.

The images present in Figures 23, 26, 29, and 32 reveal that as ram speed and extrusion ratio increases the existence of large, highly deformed grains within the shear zone begins to decrease at 25% completion. However, actual extruded lengths must be taken into account as the percentage extruded for 25% completion samples ranged from 23% to 33%. This variation in percentage extruded may have a large effect on the grain structures shown.

Figure 23: LOM collage from die face of sample 885 revealing dead metal zone and highly deformed grains within the shear zone.

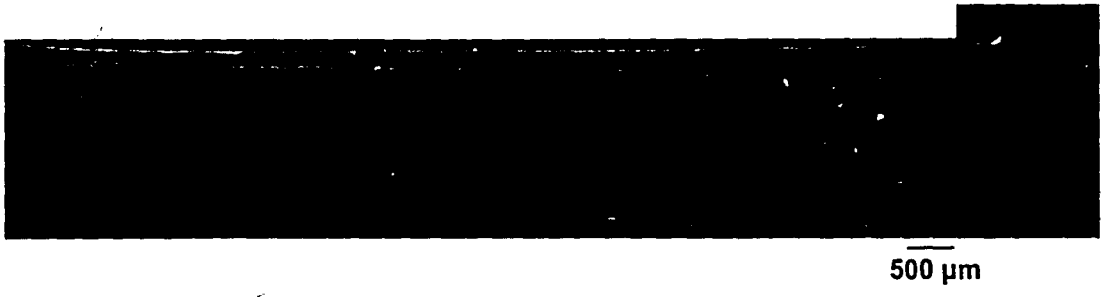

Figure 24: LOM collage from die face of sample 880 presenting dead metal zone and banded grains within shear zone.

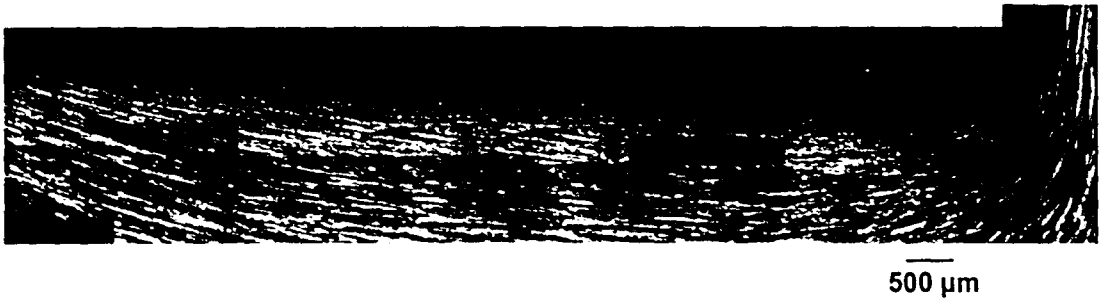

Figure 25: LOM collage from die face of sample 883 presenting dead metal zone and highly banded shear zone.

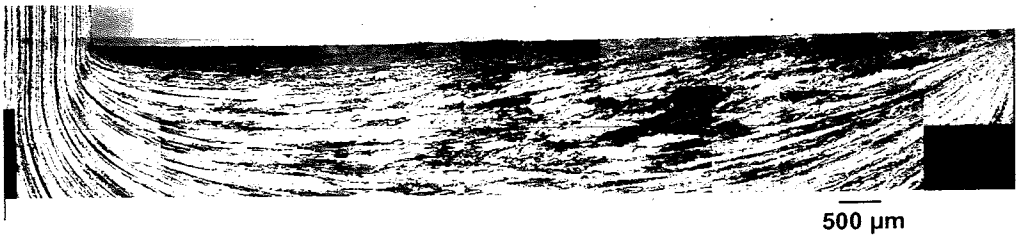

Figure 23: LOM collage from die face of sample 885 revealing dead metal zone and highly deformed grains within the shear zone.

Figure 24: LOM collage from die face of sample 880 presenting dead metal zone and banded grains within shear zone.

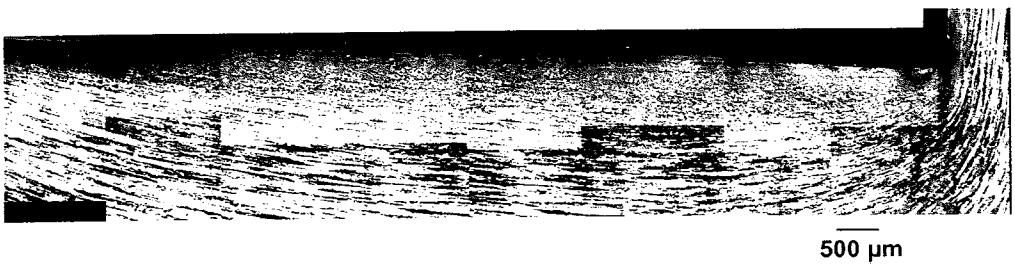

Figure 25: LOM collage from die face of sample 883 presenting dead metal zone and highly banded shear zone.

Figure 26: LOM collage from die face of sample 891 revealing dead metal zone and highly deformed grains within shear zone.

Figure 27: LOM collage from die face of sample 889 revealing dead metal zone and shear zone containing highly banded grains.

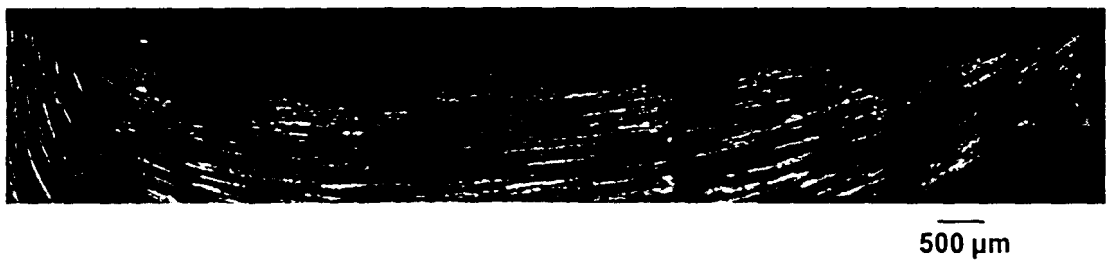

Figure 28: LOM collage from die face of sample 887 presenting dead metal zone and shear zone containing highly banded grains.

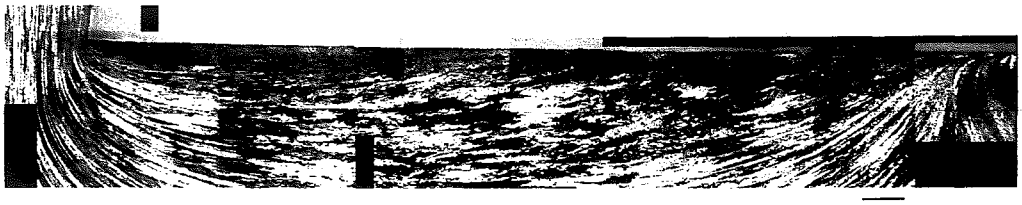

Figure 26: LOM collage from die face of sample 891 revealing dead metal zone and highly deformed grains within shear zone.

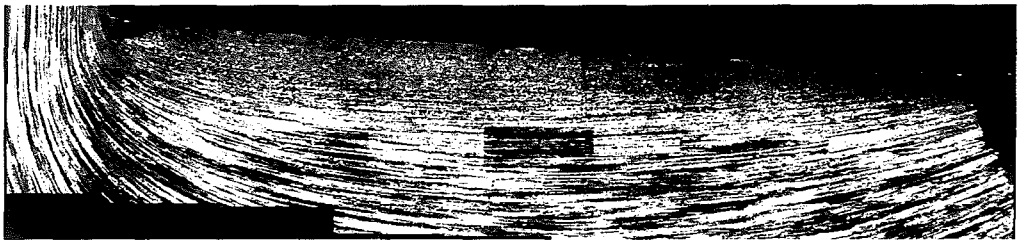

Figure 27: LOM collage from die face of sample 889 revealing dead metal zone and shear zone containing highly banded grains.

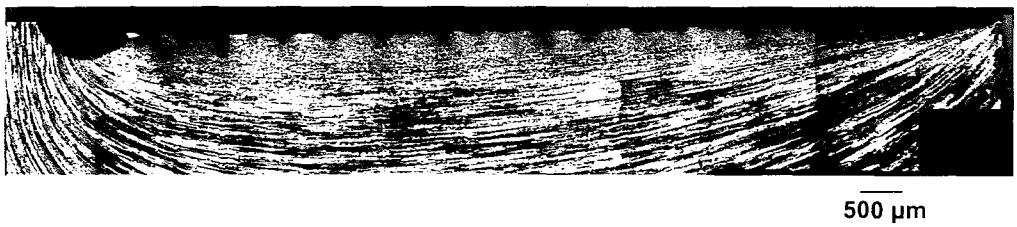

Figure 28: LOM collage from die face of sample 887 presenting dead metal zone and shear zone containing highly banded grains.

Figure 29: LOM collage from die face of sample 884 presenting dead metal zone and shear zone containing highly deformed grains.

Figure 30: LOM collage from die face of sample 879 presenting dead metal zone and shear zone containing highly banded grains.

Figure 31: LOM collage from die face of sample 881 presenting dead metal zone and shear zone containing highly banded grains.

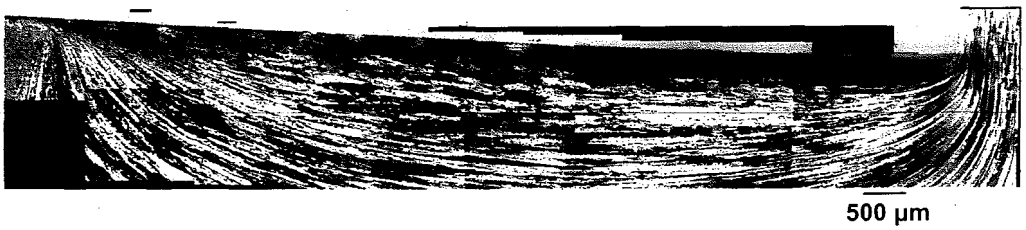

Figure 29: LOM collage from die face of sample 884 presenting dead metal zone and shear zone containing highly deformed grains.

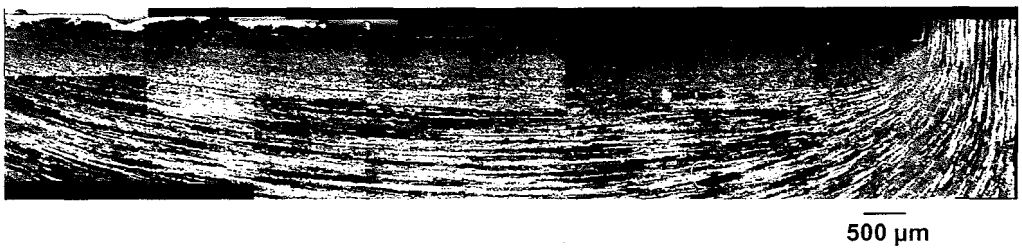

Figure 30: LOM collage from die face of sample 879 presenting dead metal zone and shear zone containing highly banded grains.

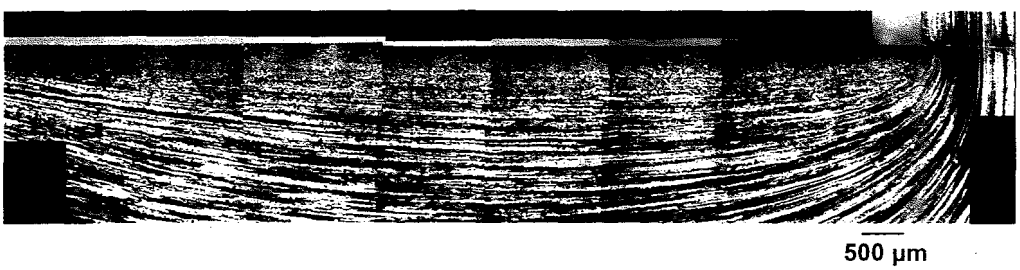

Figure 31: LOM collage from die face of sample 881 presenting dead metal zone and shear zone containing highly banded grains.

Figure 32: LOM collage from die face of sample 890 revealing dead metal zone and shear zone.

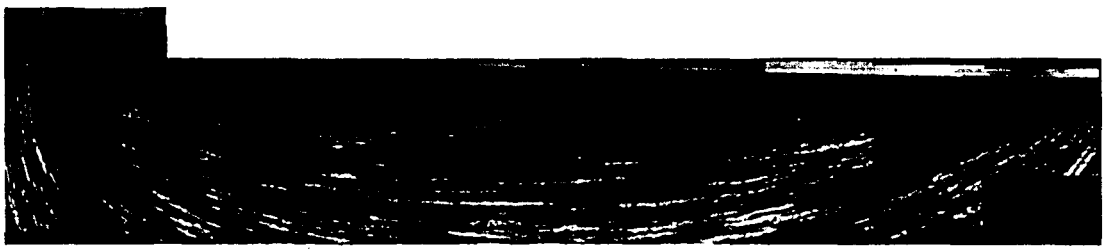

Figure 33: LOM collage from die face of sample 893 revealing dead metal zone and shear zone containing highly banded grains.

Figure 34: LOM collage from die face of sample 886 presenting dead metal zone and shear zone containing highly banded grains.

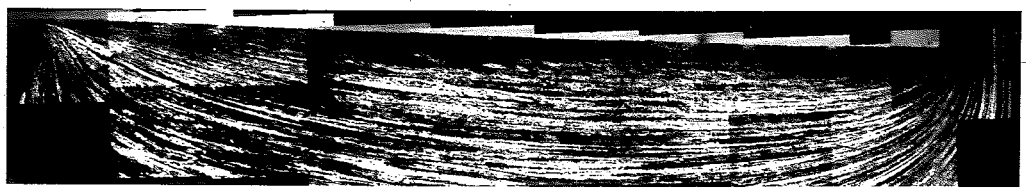

Figure 32: LOM collage from die face of sample 890 revealing dead metal zone and shear zone.

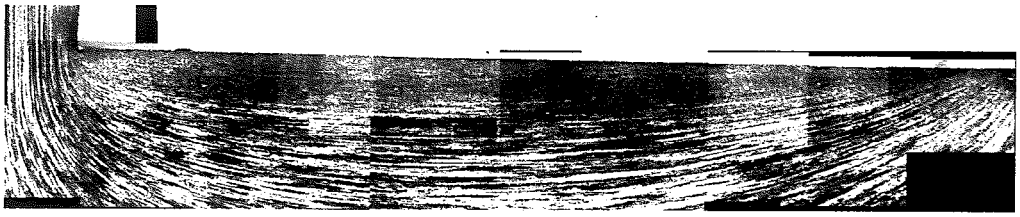

Figure 33: LOM collage from die face of sample 893 revealing dead metal zone and shear zone containing highly banded grains.

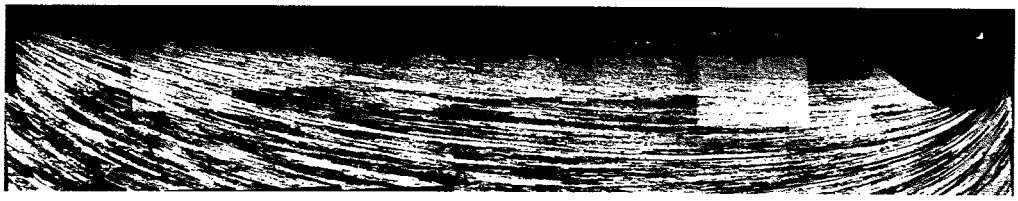

Figure 34: LOM collage from die face of sample 886 presenting dead metal zone and shear zone containing highly banded grains.

Figure 35: LOM collage from die face of low chromium sample 895 revealing dead metal zone and highly banded shear zone.

Figure 36: LOM collage from die face of low chromium sample 896 presenting dead metal zone and highly banded shear zone.

Figure 35: LOM collage from die face of low chromium sample 895 revealing dead metal zone and highly banded shear zone.

Figure 36: LOM collage from die face of low chromium sample 896 presenting dead metal zone and highly banded shear zone.

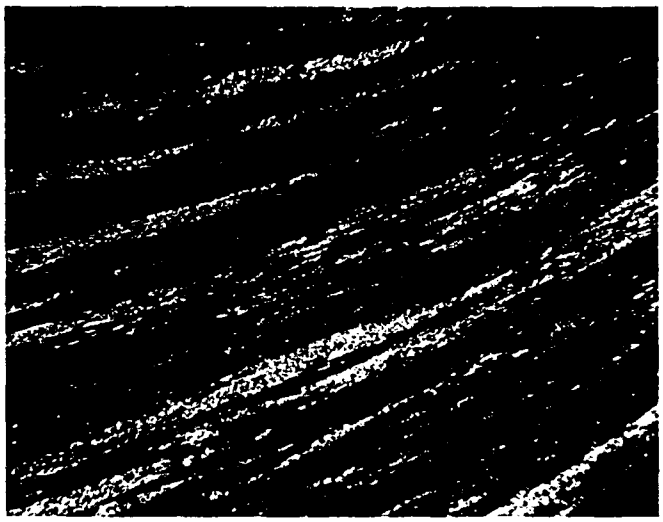

Figure 37: Image taken near die corner of extrusion discard for sample 883 revealing highly serrated and fragmented grains.

3.2.2 Extrudate Microstructures

Micrographs of the extrudates were taken to compare recrystallized depths with previously performed tests using the same processing conditions. Extrusions from parallel research were quenched with a forced air quench [12] whereas the present extrudates were quenched with a water mist. Images were taken only from 75% samples as microstructures shown here should be representative of the extrudate microstructures for 25% and 50% samples for the same testing conditions during steady state extrusion. Figures 38-41 reveal examples of extrudate microstructures taken from the die exit and extrudate for 75% extruded samples during steady state. PCG structure was not observed to form for samples 887 and 896. The surface of samples 887 and 896 contained fine equiaxed grains along with thin deformed bands.

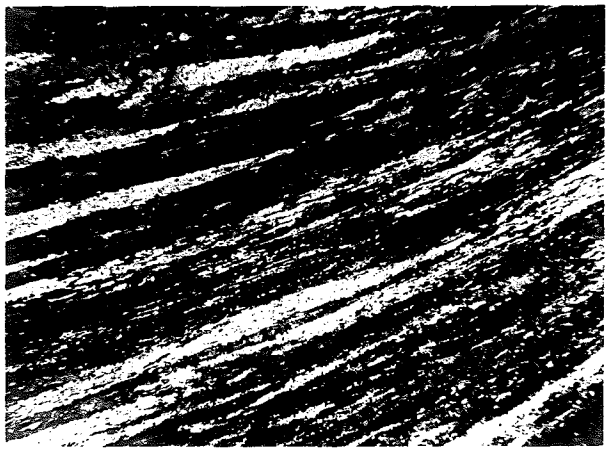

Figure 37: Image taken near die corner of extrusion discard for sample 883 revealing highly serrated and fragmented grains.

3.2.2 Extrudate Microstructures

Micrographs of the extrudates were taken to compare recrystallized depths with previously performed tests using the same processing conditions. Extrusions from parallel research were quenched with a forced air quench [12] whereas the present extrudates were quenched with a water mist. Images were taken only from 75% samples as microstructures shown here should be representative of the extrudate microstructures for 25% and 50% samples for the same testing conditions during steady state extrusion. Figures 38-41 reveal examples of extrudate microstructures taken from the die exit and extrudate for 75% extruded samples during steady state. PCG structure was not observed to form for samples 887 and 896. The surface of samples 887 and 896 contained fine equiaxed grains along with thin deformed bands.

Figures 39 and 40 reveal extrudate microstructures immediately after the die exit. No PCG formation was witnessed in these samples. Therefore, the PCG structure witnessed in Figures 38 and 40 is understood to have formed after significant time after exiting the die.

Figure 38: Extrudate micrograph of sample 881 extruded at 400°C with a strain rate of 2.6mm/s and extrusion ratio of 40 revealing PCG at the extrudate surface and few recrystallized grains within the deformed region.

Figures 39 and 40 reveal extrudate microstructures immediately after the die exit. No PCG formation was witnessed in these samples. Therefore, the PCG structure witnessed in Figures 38 and 40 is understood to have formed after significant time after exiting the die.

Figure 38: Extrudate micrograph of sample 881 extruded at 400°C with a strain rate of 2.6mm/s and extrusion ratio of 40 revealing PCG at the extrudate surface and few recrystallized grains within the deformed region.

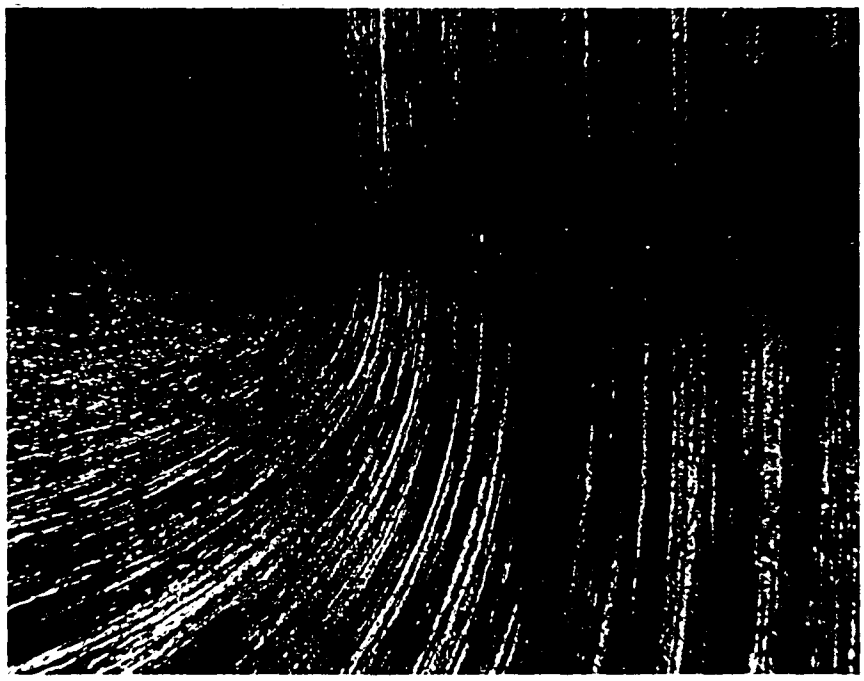

Figure 39: LOM micrograph of sample 881 taken at die exit revealing no PCG at surface immediately after exiting the die. (Crack at die exit is the result of removal from tooling)

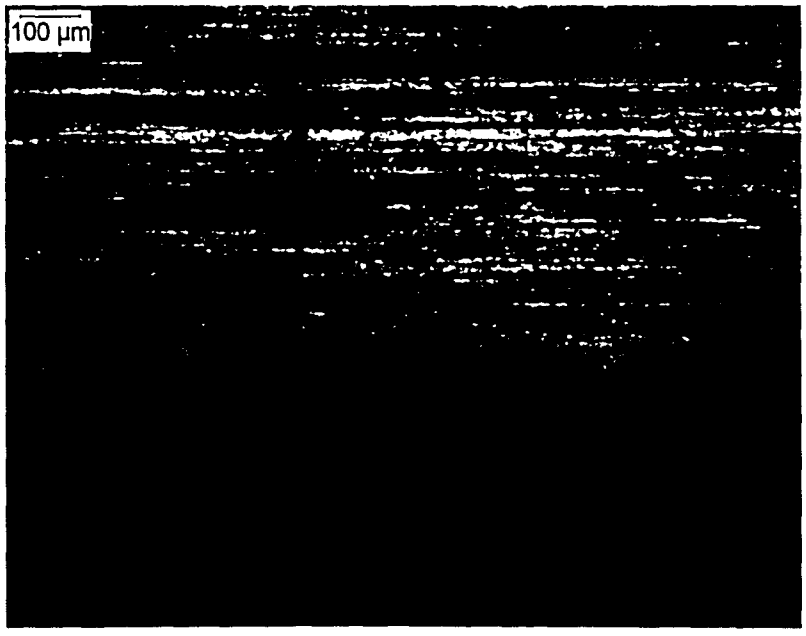

Figure 40: Extrudate micrograph of surface region of sample 883 extruded at 400°C with a strain rate of 2.6mm/s and extrusion ratio of 20 revealing a strong delineation between surface PCG and deformed bands.

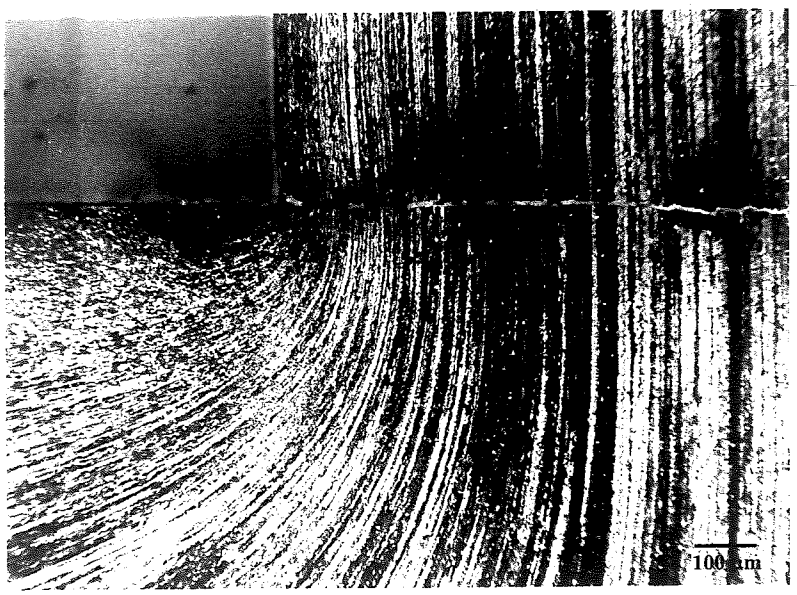

Figure 39: LOM micrograph of sample 881 taken at die exit revealing no PCG at surface immediately after exiting the die. (Crack at die exit is the result of removal from tooling)

Figure 40: Extrudate micrograph of surface region of sample 883 extruded at 400°C with a strain rate of 2.6mm/s and extrusion ratio of 20 revealing a strong delineation between surface PCG and deformed bands.

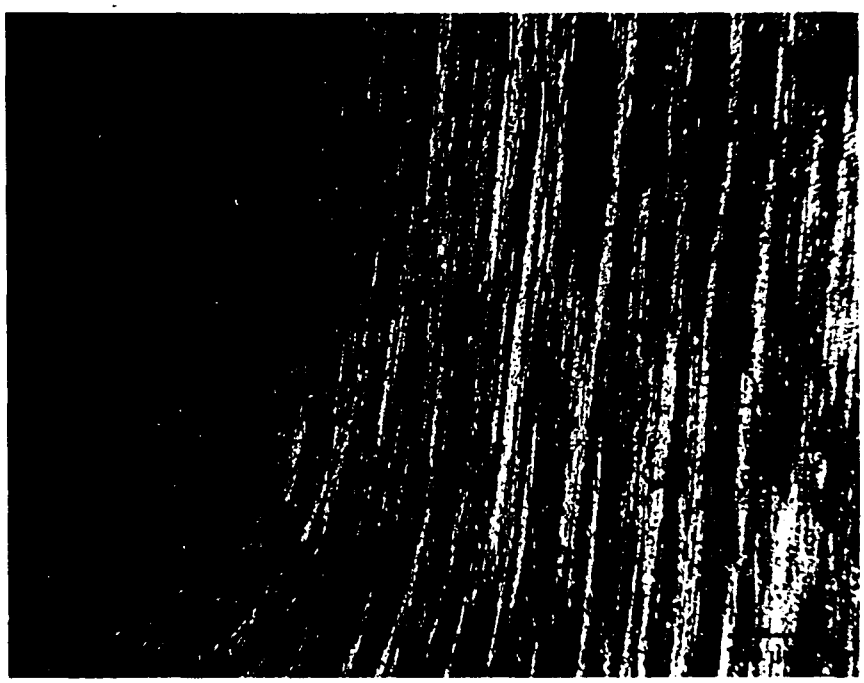

Figure 41: LOM micrograph of sample 883 taken at die exit revealing no PCG at extrudate surface immediately after exiting the die.

3.2.3 EBSD Analysis of Billet Discards

EBSD was performed on the billet discards of samples 880, 883, and 885. Scans were taken at the estimated transition of dead metal to shear zone as dictated by LOM. Orientation maps obtained for each sample across the die face can be seen in Figures 42-44. The evolution of microstructure from the die face (dead metal zone) into the shear zone from 25% to 75% completion was easily resolved using EBSD. In samples 883 and 885 representing 75% and 50% completion, the observed microstructural gradients from the die face into the billet were extremely similar. Within the dead metal zone, fine equiaxed grains of high misorientation ranging in

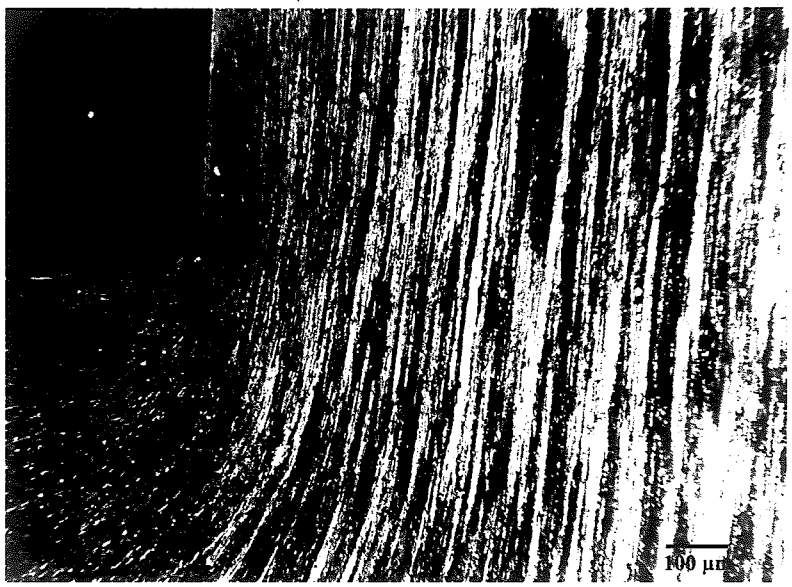

Figure 41: LOM micrograph of sample 883 taken at die exit revealing no PCG at extrudate surface immediately after exiting the die.

3.2.3 EBSD Analysis of Billet Discards

EBSD was performed on the billet discards of samples 880, 883, and 885. Scans were taken at the estimated transition of dead metal to shear zone as dictated by LOM. Orientation maps obtained for each sample across the die face can be seen in Figures 42-44. The evolution of microstructure from the die face (dead metal zone) into the shear zone from 25% to 75% completion was easily resolved using EBSD. In samples 883 and 885 representing 75% and 50% completion, the observed microstructural gradients from the die face into the billet were extremely similar. Within the dead metal zone, fine equiaxed grains of high misorientation ranging in

size from 2 to 10 μm were observed. Continuing into the billet, elongated highly misoriented grains were found to be interspersed with fine grains similar to those within the dead metal zone. These banded grains become more continuous deeper into the billet indicated the complete transition to the shear zone. These three areas are indicated in Figure 42 labeled 1-3 respectively. Figures 42 and 43 also reveal the formation of new grains both within and on the boundaries of elongated grains. This phenomena will be further discussed in the Discussion section of this thesis.

Figure 44 reveals the orientation maps obtained for 25% extruded sample 885. An obvious difference in microstructure exists for the 25% extruded sample versus the 50% and 75% samples. Sample 885 exhibited a smaller dead metal zone while the shear zone exhibited larger deformed bands than those witnessed in the 50% and 75% microstructures. Grain formation within bands and grain fragmentation was observed in the 25% sample along with highly serrated grain boundaries nearing the die orifice.

Investigation of the deformation zones within samples, 880, 883, and 885 revealed that the dead metal zone/shear zone interface was quite diffuse in most of the scans obtained. This uncertainty in the transition zone will be further discussed and dealt with in the following section.

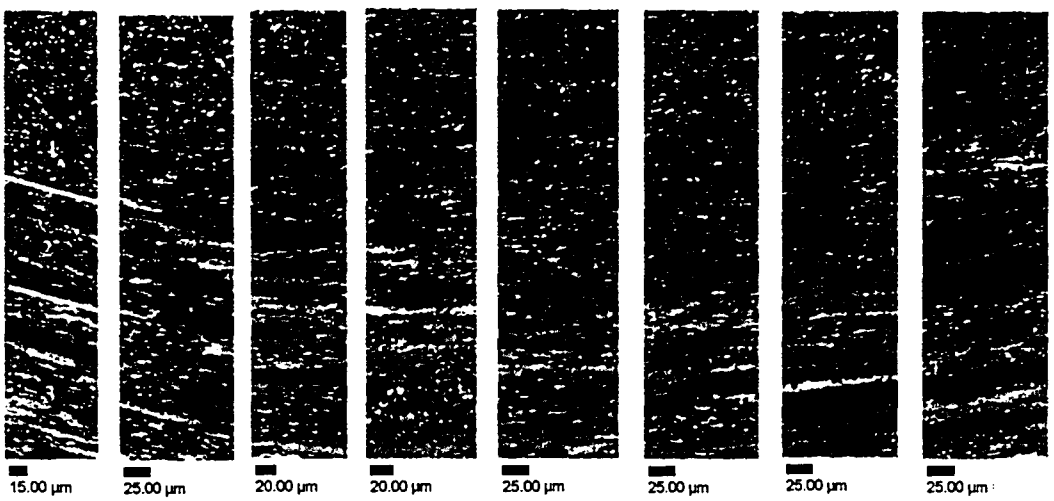

Figure 42: Orientation maps obtained for 75% extruded billet sample 883.

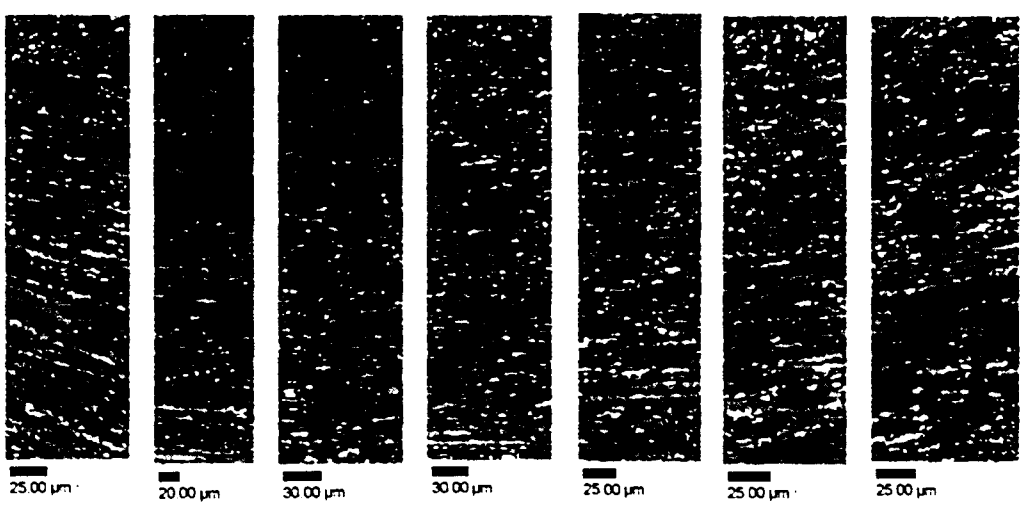

Figure 43: Orientation maps obtained for 50% extruded billet sample 880.

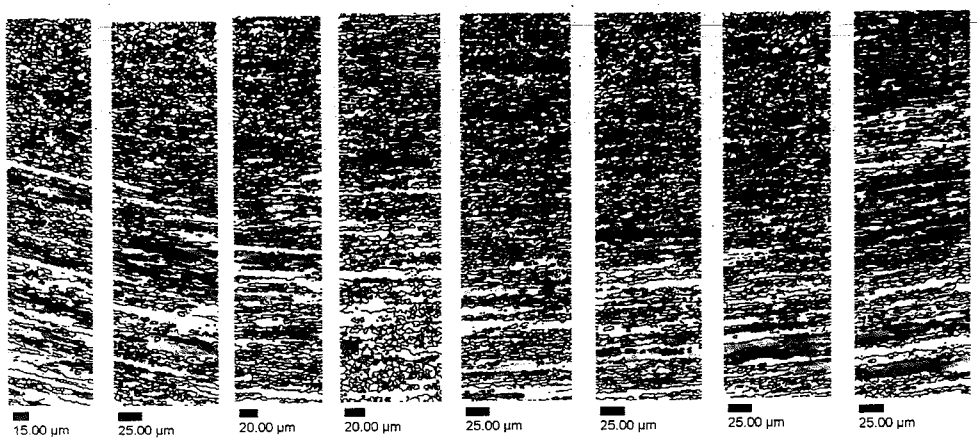

Figure 42: Orientation maps obtained for 75% extruded billet sample 883.

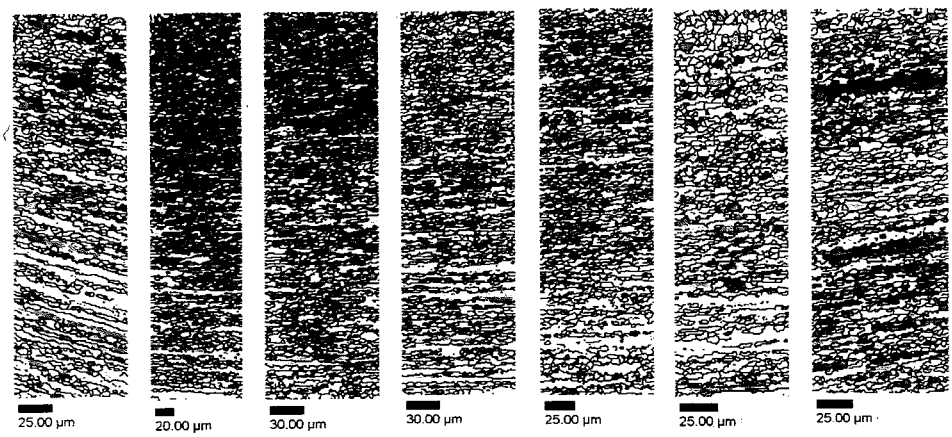

Figure 43: Orientation maps obtained for 50% extruded billet sample 880.

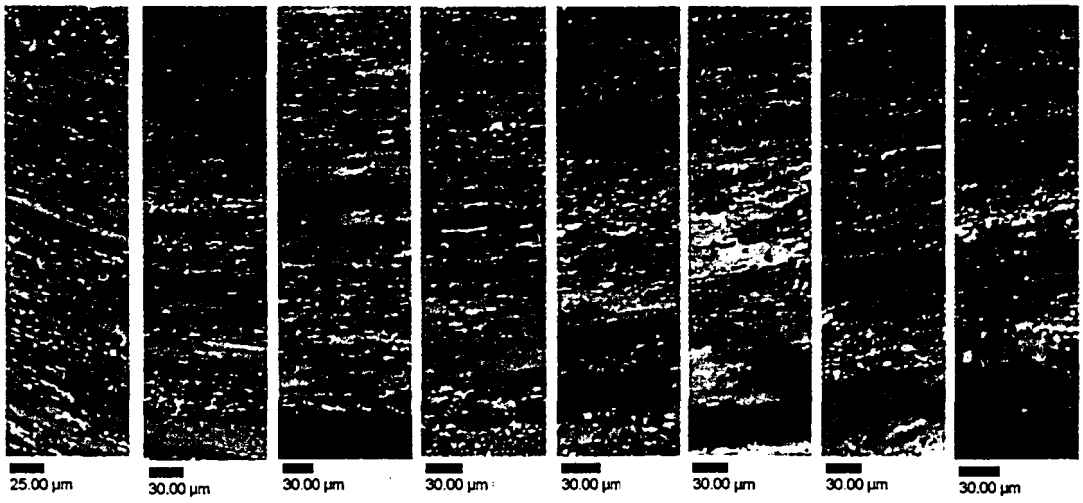

Figure 44: Orientation maps obtained for 25% extruded billet sample 885.

3.2.4 Dead Metal Zone Area Measurements

3.2.4.1 LOM Dead Metal Zone Area Measurements

In order to characterize the evolution of metal flow during indirect extrusion of 6061 aluminum, depth measurements from the die face to the end of "continuous" dead metal were taken for each partially extruded sample listed previously. Measurements were taken by two different individuals to test the accuracy of this method. Figures 45 and 46 reveal graphs of the two separate measurements taken by two different individuals for each sample. It can be seen in Figures 45 and 46 that a large variability in the selection of dead metal zone depths via LOM exists; therefore, trends relating dead metal zone depths with process parameters also varied.

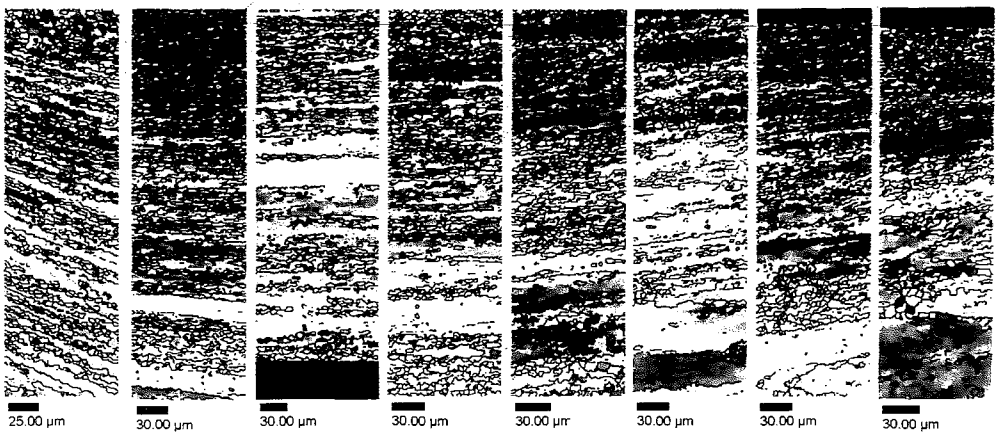

Figure 44: Orientation maps obtained for 25% extruded billet sample 885.

3.2.4 Dead Metal Zone Area Measurements

3.2.4.1 LOM Dead Metal Zone Area Measurements

In order to characterize the evolution of metal flow during indirect extrusion of 6061 aluminum, depth measurements from the die face to the end of "continuous" dead metal were taken for each partially extruded sample listed previously. Measurements were taken by two different individuals to test the accuracy of this method. Figures 45 and 46 reveal graphs of the two separate measurements taken by two different individuals for each sample. It can be seen in Figures 45 and 46 that a large variability in the selection of dead metal zone depths via LOM exists; therefore, trends relating dead metal zone depths with process parameters also varied.

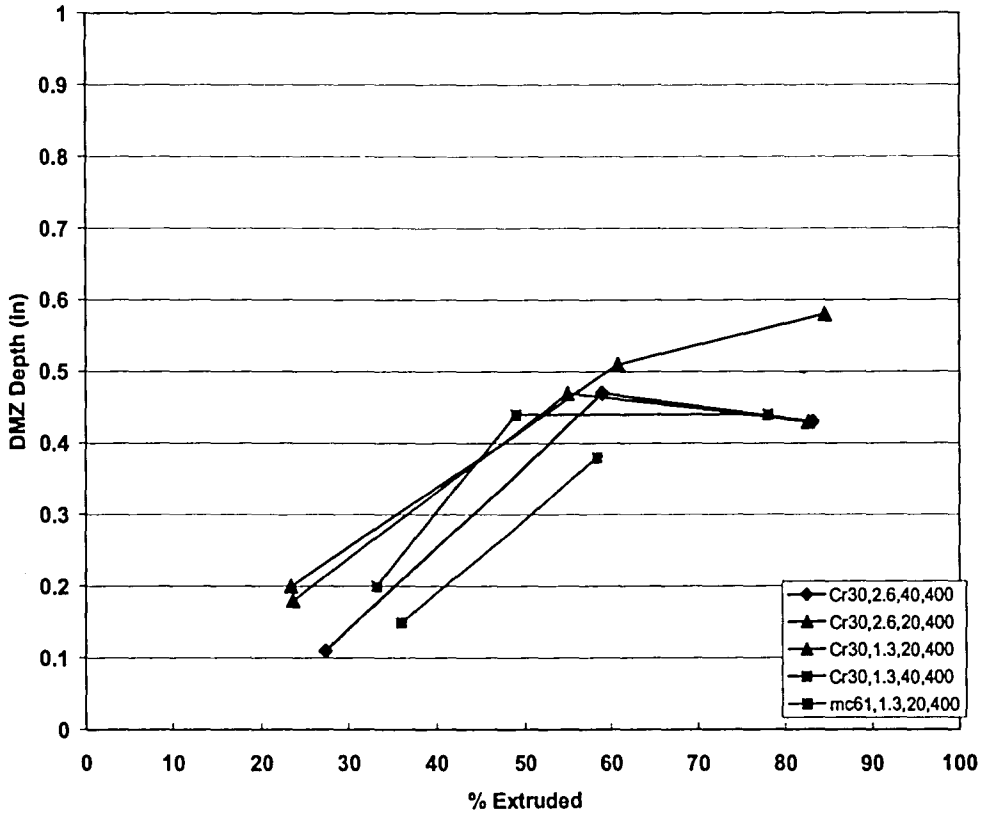

Figure 45: Plot of visual measurements taken by first individual of DMZ depth versus percentage extruded.

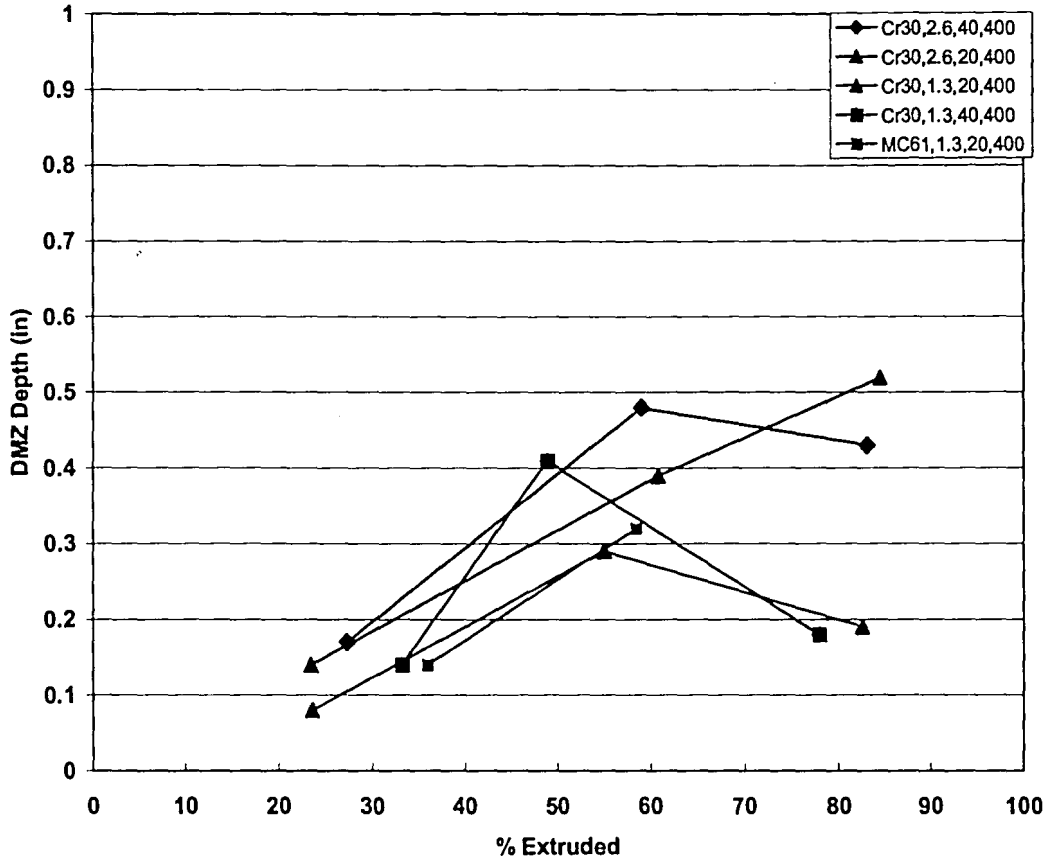

Figure 46: Plot of visual measurement taken by second individual of DMZ depth versus percentage extruded.

3.2.4.2 Grain Shape Aspect Ratio Measurements using EBSD

Grain shape aspect ratios were obtained from EBSD maps produced. It was expected that the variation in aspect ratios across the dead metal/shear zone interface would provide an accurate definition of this interface. Figure 47 shows a plot of aspect ratio versus depth from die face. Each point on the aspect ratio map corresponds to one grain on the EBSD map obtained. It can be seen in this figure

that an accurate definition of the dead metal/shear zone interface was difficult to detect due to the large presence of fine equiaxed grains throughout the scanned region.

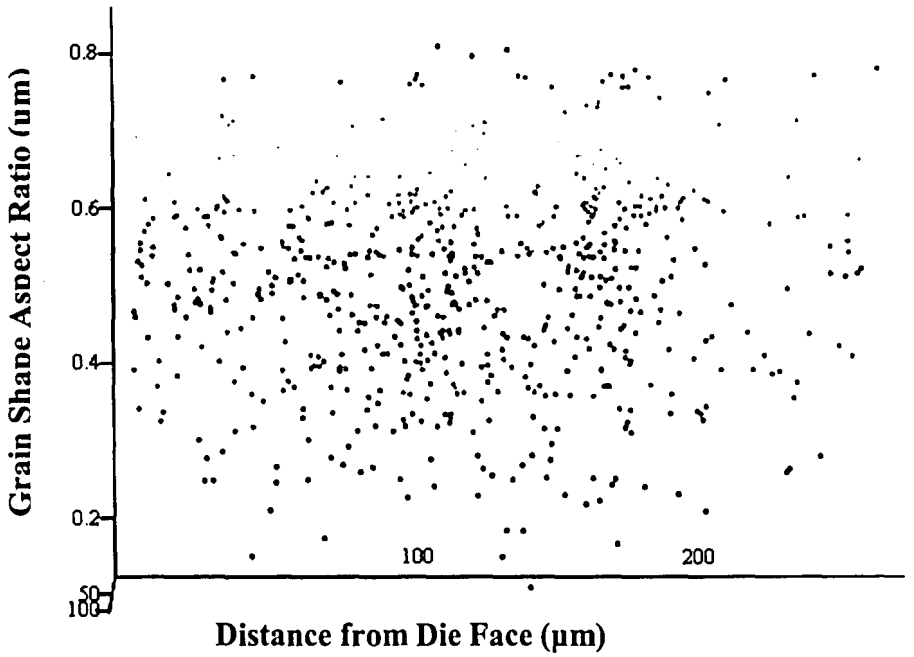

Figure 47: Plot revealing grain shape aspect ratio versus distance from die face.

3.2.4.3 Grain Size Measurements using EBSD

In order to more precisely characterize the transition from the dead metal zone to the shear zone, grain size maps, seen in Figures 48-50, were obtained for samples 880, 883 and 885. Measurements were performed on grain size maps to obtain and evaluate the evolution of dead metal, transition, and shear zones during

indirect extrusion for samples 880, 883, and 885. Data obtained on the depth of the transition zone were imported into Mathcad and Microsoft Excel software to obtain area projections and approximate geometries of the dead metal zones.

Figure 51-53 are plots of the measurements taken for each scan. Each plot contains three lines signifying the three measurement points taken per scan. The area located between the top and bottom line is defined as the transition zone between the dead metal and shear zones within each sample. It was assumed for these measurements that the transition zone extended to the die corner for the 50% and 75% samples; whereas, the transition zone ended 1mm away from the die corner for the 25% sample. These assumptions were based off LOM images and future work will need to be performed to determine the exact location of where the transition zone ends. The area of material contained within the dead metal and transition zones was obtained by two methods. First, the trapezoidal rule was applied to each graph of measurements, seen in Figures 51-53, to approximate the area bounded by the curves. Each graph contains three curves representing the measurements taken at the end of "continuous" dead metal, within the transition zone, and at the beginning of the "continuous" shear zone. Results from this method can be seen in Table VII. Area measurements obtained from the trapezoidal rule generally revealed that as extrusion progresses from 25-75% completion, the area of material contained in the "continuous" dead metal zone increased substantially.

Table VII also reveals area measurements obtained from a least squares fit calculation through measurement points obtained. Results again indicate an increase

in material contained within the "continuous" dead metal zone as extrusion progresses from 25-75% completion. There exists a slight difference in the area measurements obtained. This difference is due to the inherent error in using both of these methods to calculate area. Thus it must be noted that these measurements are approximations of the dead metal zone area.

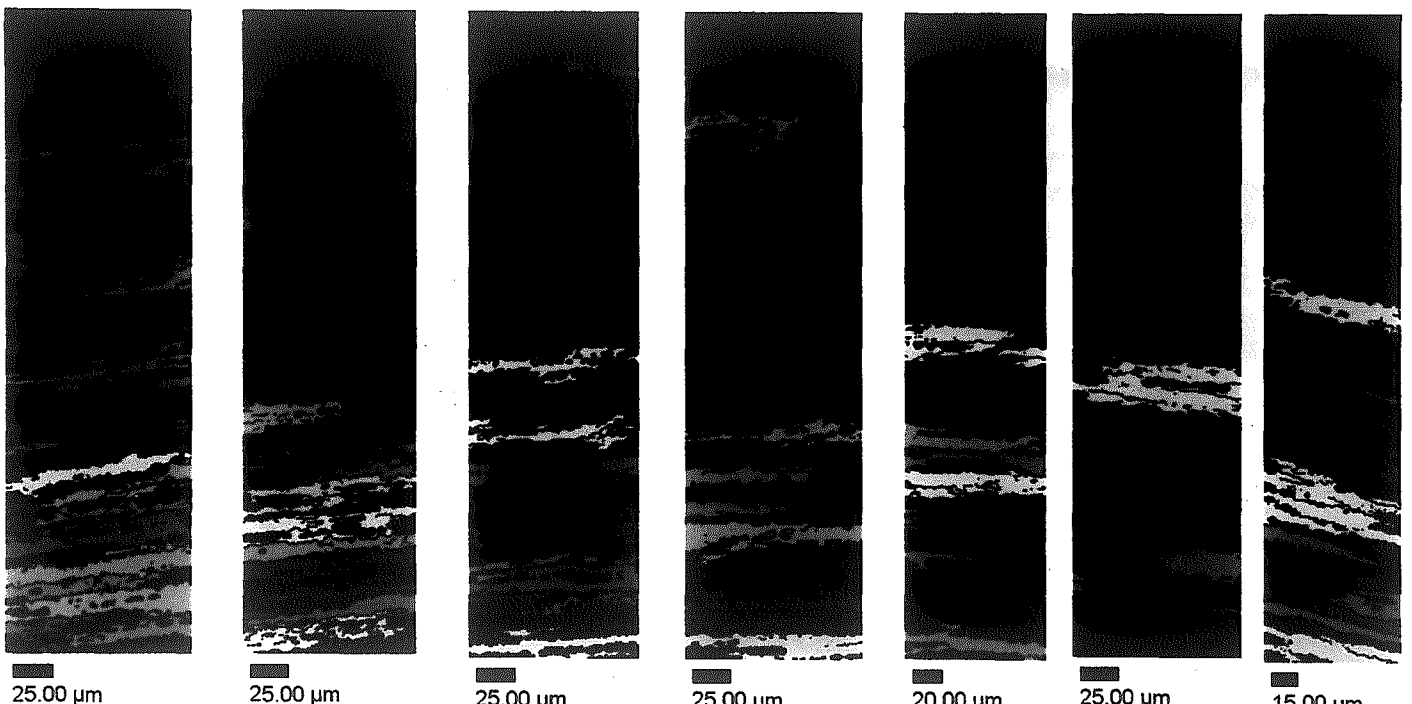

Figure 48: Grain size maps taken across die face of 75% partially extruded sample 883.

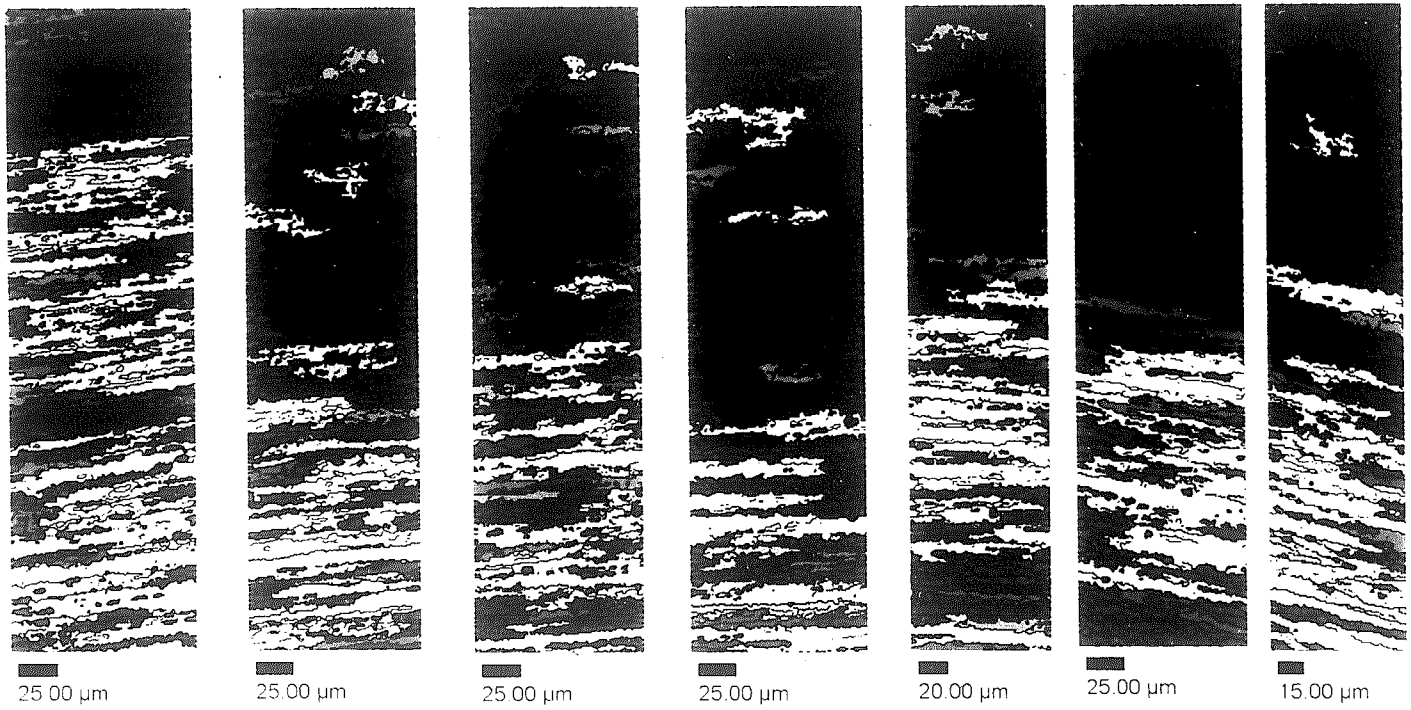

Figure 48: Grain size maps taken across die face of 75% partially extruded sample 883.

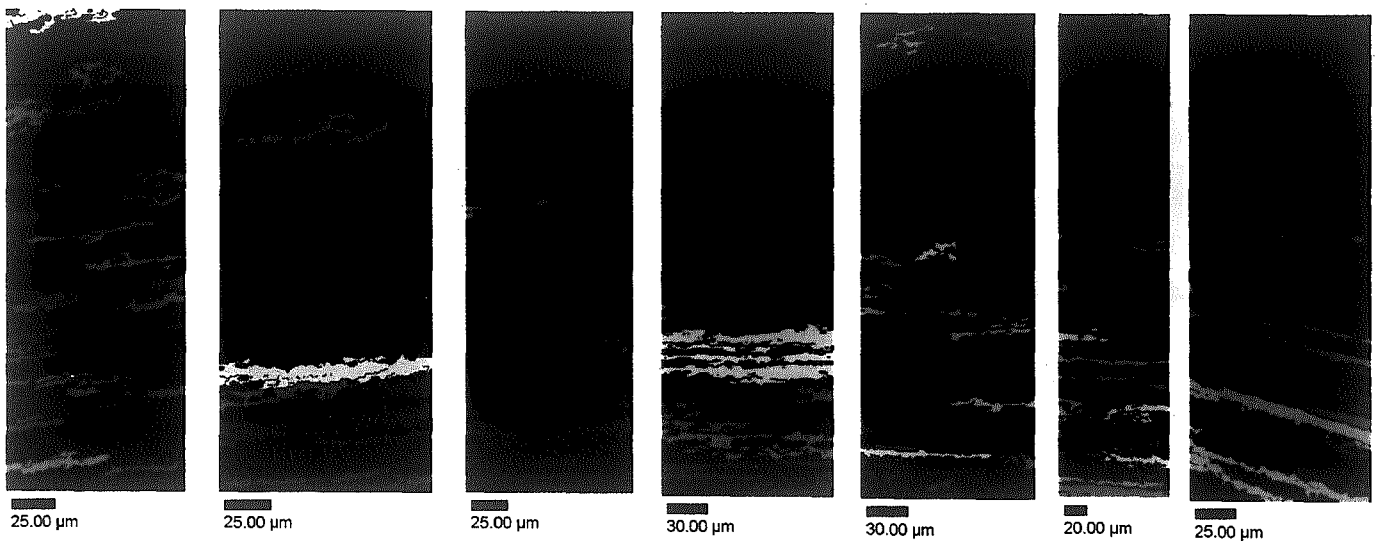

Figure 49: Grain size maps taken across die face of 50% partially extruded sample 883.

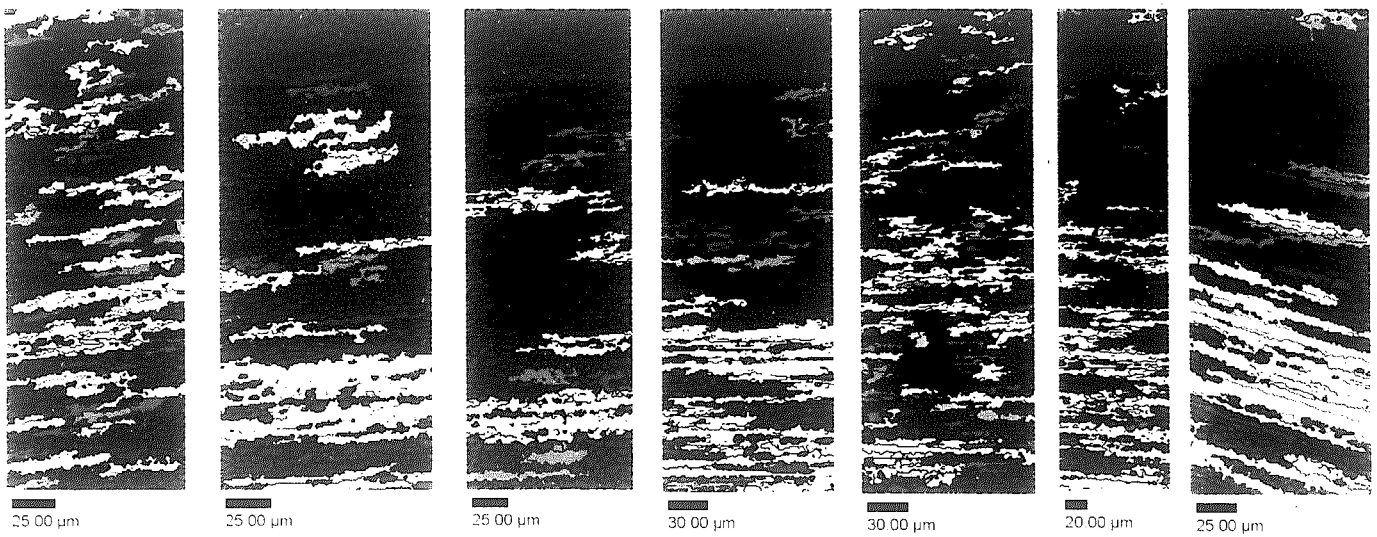

Figure 49: Grain size maps taken across die face of 50% partially extruded sample 883.

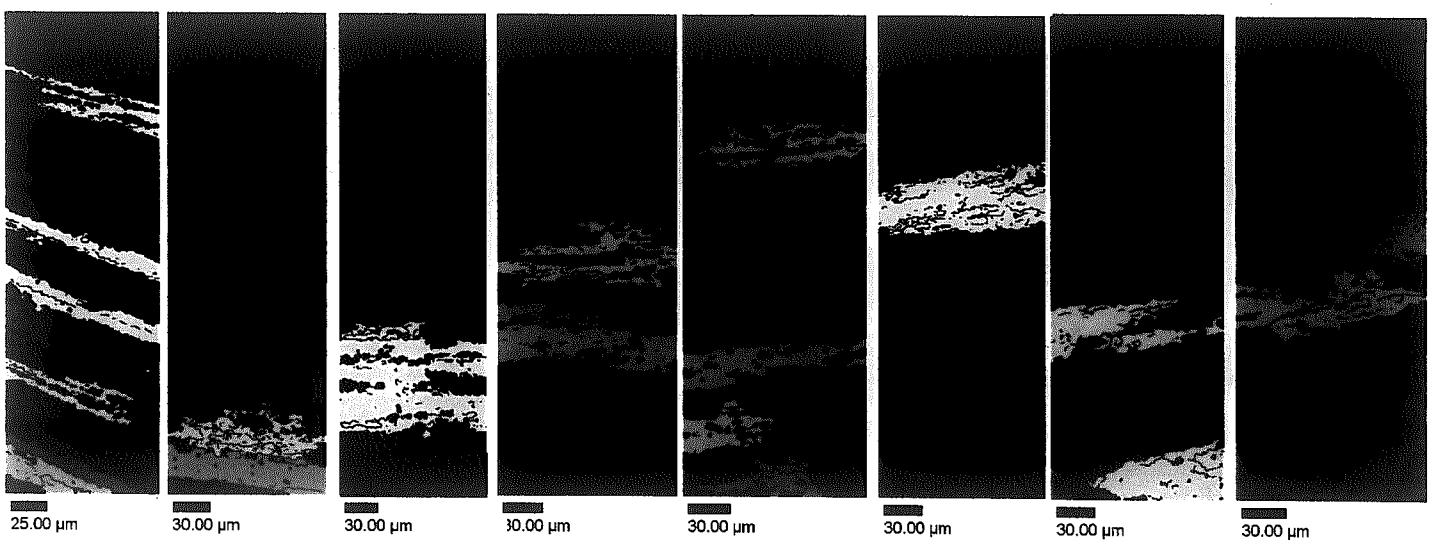

Figure 50: Grain size maps performed across die face on 25% partially extruded sample 885.

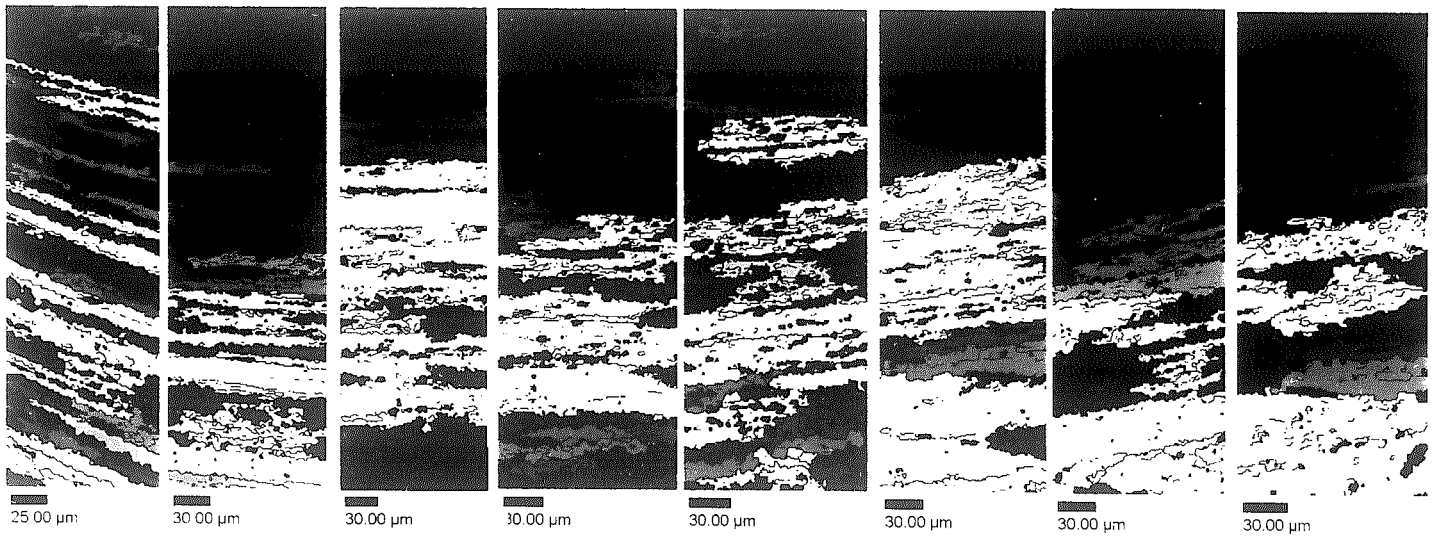

Figure 50: Grain size maps performed across die face on 25% partially extruded sample 885.

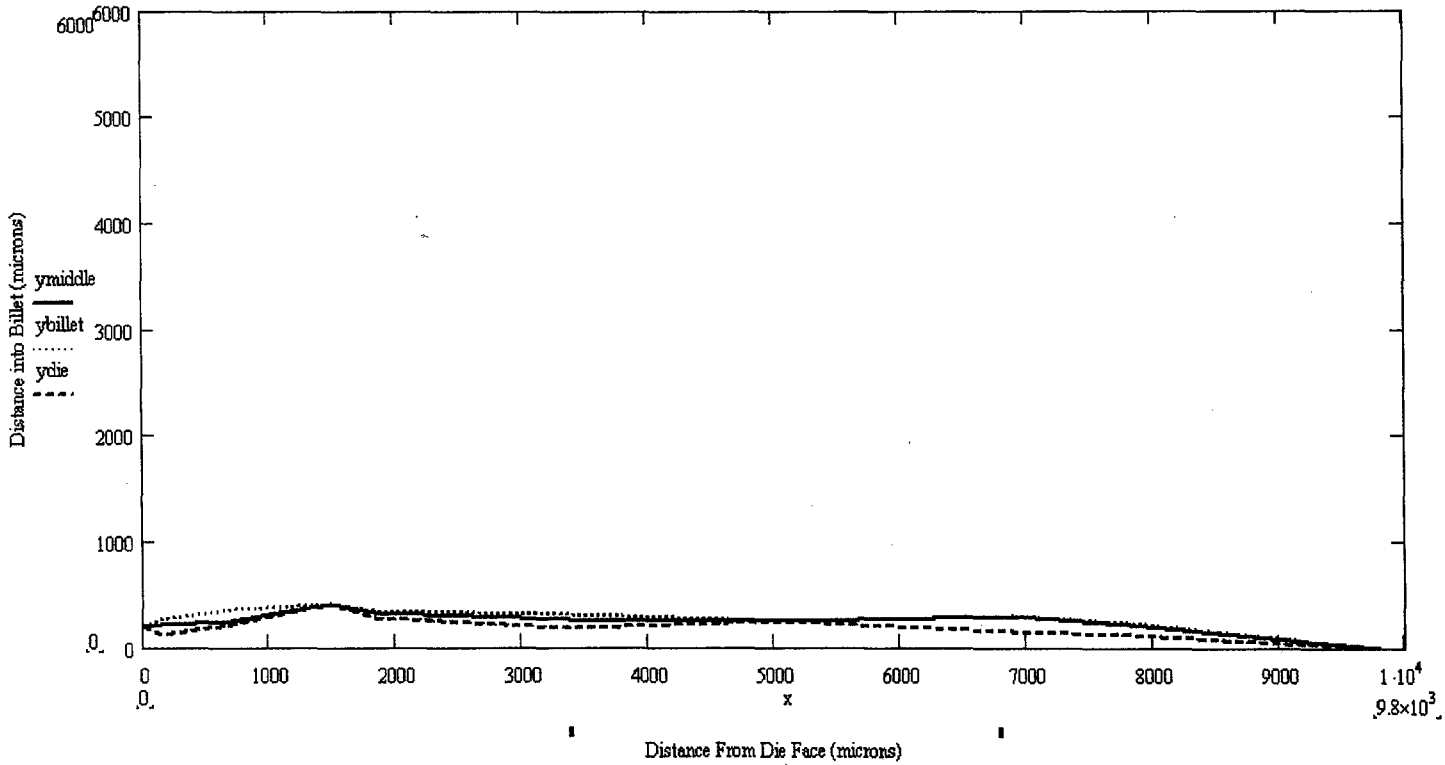

Figure 51: Plot of actual DMZ measurements for 25% sample revealing transition zone.

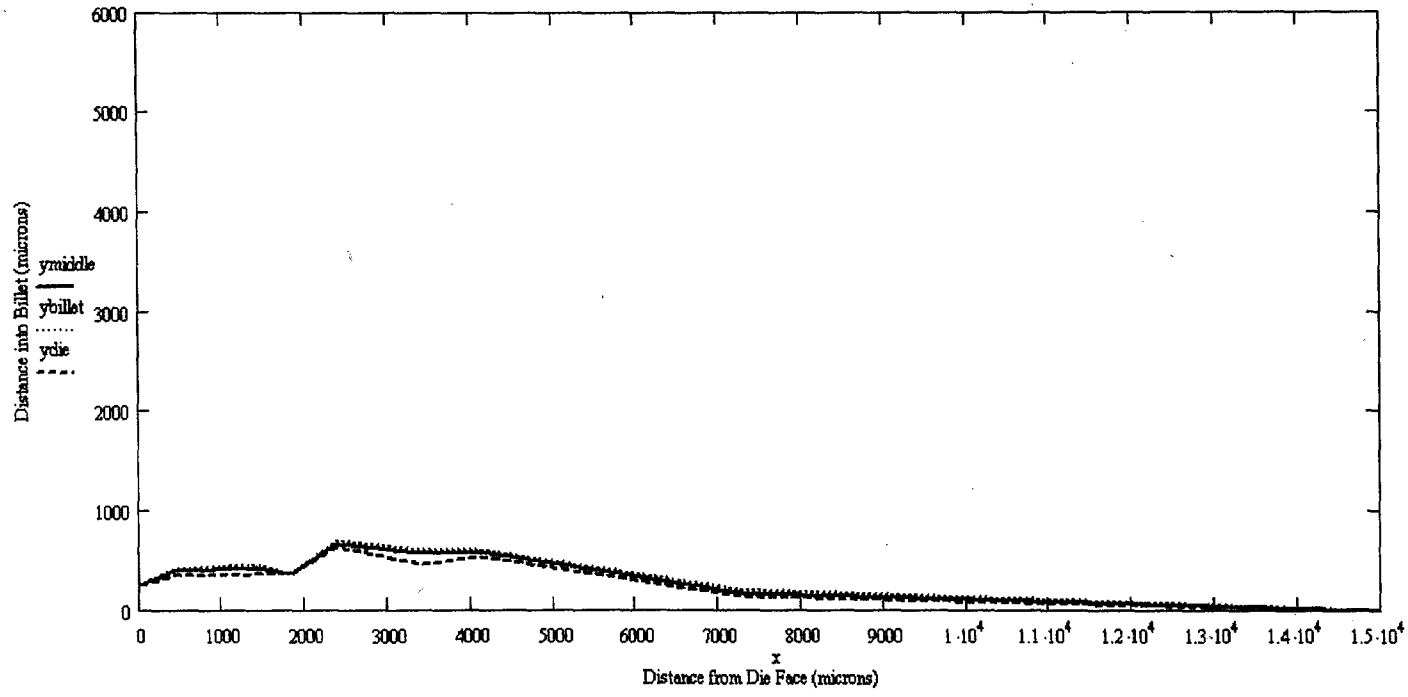

Figure 52: Plot of actual dead metal zone measurements from EBSD grain size maps for 50% sample revealing transition zone.

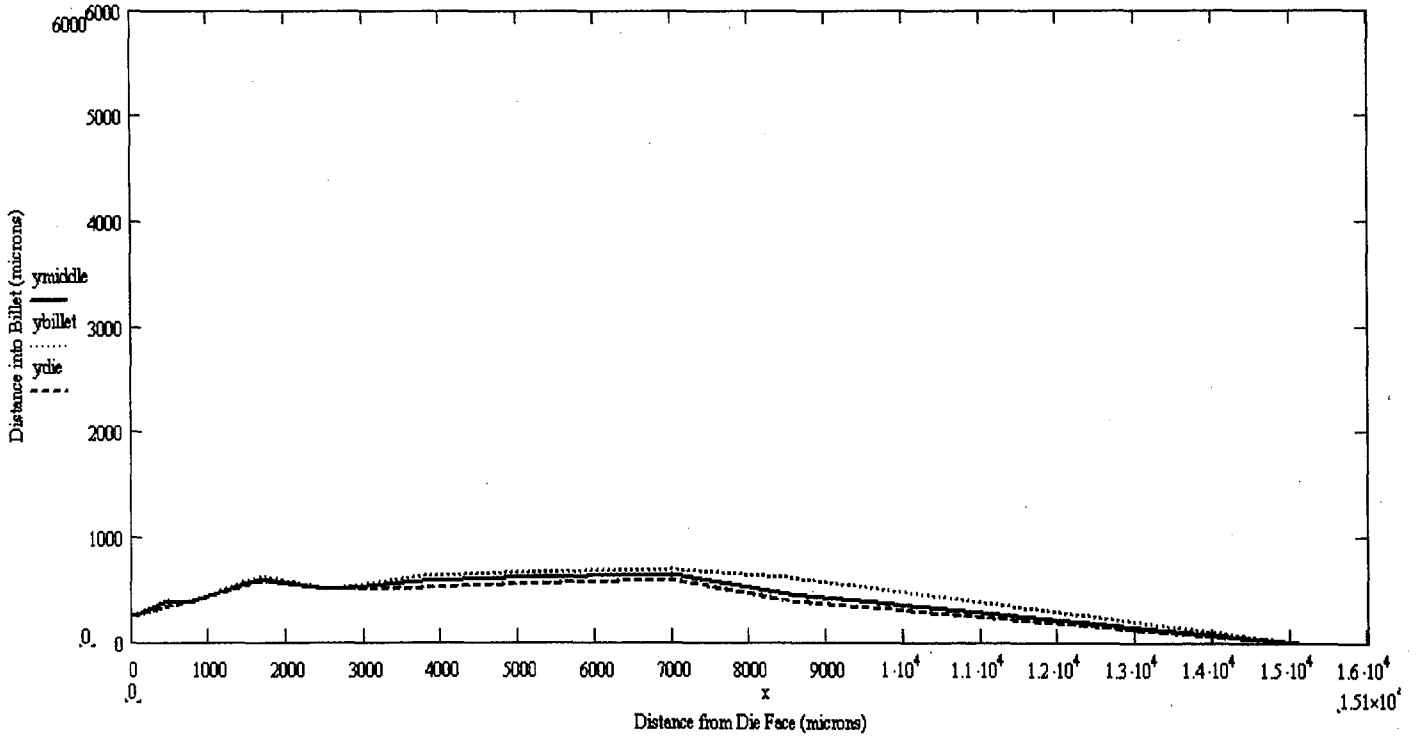

Figure 53: Plot of actual DMZ measurements for 75% sample revealing transition zone.

Table VII: Area measurements for 25, 50, and 75% samples obtained through trapezoidal rule and least squares fit calculations.

Percent Completion	Trapezoidal Rule "Continuous" DMZ $(\mu m)^2$	Trapezoidal Rule Transition Zone $(\mu m)^2$	Trapezoidal Rule Shear Zone $(\mu m)^2$	Least Squares Fit "Continuous" Dead Metal Area $(\mu m)^2$
25	2.082×10^6	2.843×10^6	3.124×10^6	4.034×10^6
50	3.397×10^6	3.833×10^6	4.123×10^6	5.132×10^6
75	5.669×10^6	6.161×10^6	7.053×10^6	6.188×10^6

4.0 DISCUSSION

4.1 Billet Microstructure Evolution

Understanding the evolution of billet microstructure during extrusion of 6061 is crucial to predicting and controlling final extrudate microstructure. Previous research investigating PCG formation in 6061 aluminum indirect extrusions provided the foundation for the present research [27]. Testing parameters utilized in this research were based upon previously reported results on reduced PCG depth [12]. Small-scale indirect extrusions were performed on two versions of 6061 alloys, high and low chromium. Low chromium 6061 aluminum alloys, however, were not of great importance to the current research as they were extruded merely as a standard for comparison. Therefore, all analyses were performed on high chromium 6061 aluminum alloy material. Only one deformation temperature was utilized as previous results indicated a reduction in PCG at lower deformation temperatures. The deformation temperature used in the analyzed experiments is one typically experienced in industrial practice.

LOM and EBSD analysis of partially extruded 6061 billets revealed a distinct variation in billet microstructure near the die face from 25% to 75% completion. Each series of samples for all testing conditions exhibited three distinct regions: a dead metal zone, a transition zone, and shear zone. Dead metal zones and shear zones are expected to occur during indirect extrusion of aluminum alloys as was

described earlier. The transition zone has been introduced in this thesis to define the area between "continuous" dead metal and "continuous" deformed metal. Much debate exists on whether the metal within the dead metal zone is not stagnant during indirect extrusion, or whether a traditional dead metal zone actually forms. The results presented in this thesis suggest that the dead metal zone witnessed is not completely stagnant, but, instead undergoes some strain causing the microstructure within this region to vary during the extrusion process. Friction conditions at the die surface may, however, cause grains directly at the die face to remain stationary. Results from LOM and EBSD also demonstrated a diffuse dead metal/shear zone interface. The ambiguity surrounding this interface or transition zone, which was observable with both LOM and EBSD, further supports that the dead metal/shear zone interface is constantly changing its geometry as deformation proceeds.

Investigation of grain morphology within these zones has given evidence of the evolution of billet microstructure, specifically the dead metal zone near the die face. Dead metal zones within all samples contained a fine structure that was not resolvable using LOM. LOM observation, however, did reveal that among samples extruded to the same percent completion, the metal flow patterns within the deformation zone were analogous despite variations in testing parameters. Due to this fact, one series of samples (880, 883, and 885) was chosen for EBSD. It is assumed that the microstructural gradients revealed from EBSD analysis of these three samples is representative of gradients present in samples extruded under varying testing parameters. It must be noted, however, that slight microstructural

differences may actually exist among samples with varying testing parameters due to variations in strain gradients across the billet. For the purposes of this research, it is assumed that the observed microstructural gradients would be present in all samples. Further work will need to be performed on remaining partially extruded samples to investigate if there is an effect of extrusion testing parameters on the volume of dead metal during indirect extrusion.

Results of LOM analysis did indicate that the existence of large deformed grains within the shear zone of 25% partially extruded samples decreased with increasing extrusion ratio and ram speed. Results from these samples also revealed that the actual percentage extruded varied from the programmed 25%. This microstructural variation between 25% samples may be attributed to their actual extruded percentages as high strain samples exhibiting a decrease were extruded to 27% and 33% completion versus 23% for both the lower strain samples. Therefore, it must be noted that this distinct difference in grain structures between the high strain (R = 40) and low strain samples (R = 20) may be the natural progression of the dead metal and shear zones during indirect extrusion.

EBSD analysis confirmed the existence of fine, equiaxed, highly-misoriented grains within the dead metal zone of 25, 50 and 75% extruded samples. Within the transition zone and shear zone, high angle, equiaxed fine grains were also witnessed to form both within elongated grains, as well as, in the vicinity of deformed grains with highly serrated grain boundaries. Fragmented grains or "pinched-off" grains were witnessed to form in the transition and shear zones across the entire die face. In

25% extruded samples, this transition zone was later found to evolve into the dead metal zone of 50 and 75% extruded samples further suggesting that the formation of dead metal zone grains occurs by the fragmentation of previous high angle grains from highly deformed elongated grains.

Along with grain formation and fragmentation, deformed bands within the shear zone decreased in size from 25% to 75% extrusion. This evolution is expected as banded grains undergo continuing strain during the extrusion process. As elongated grains continue to deform during the extrusion process, as can be seen in Figures 42-44, serrations were witnessed to develop along grain boundaries. In some instances, evidence of larger deformed grains with major axes on the order of 20 μm were found within the "continuous" dead metal zone to contain grain boundary serrations nearing impingement. An example of this microstructural feature can be seen in Figure 49. For the 25% sample, these serrations were exaggerated closer to the die orifice suggesting serrations in grain boundaries are an affect of the strain induced on a grain during deformation.

The grain formation and fragmentation and grain boundary serrations witnessed in these samples may be attributed to a continuous dynamic recrystallization process such as geometric dynamic recrystallization (gDRX). gDRX occurs when new, high-angle grains form as a result of the impingement of previous high angle grain boundaries with either subgrain boundaries or other high angle grain boundaries during deformation. Microstructures resulting from gDRX, such as that shown in Figure 11, strongly resemble those found within the dead metal

zones studied in the current work. It must be noted, however, that billet discards were quenched within 35 seconds after completion of extrusion. Due to this time delay, the high angle, fine, equiaxed grains witnessed could also be the result of a static recrystallization process.

Investigation of the structure near the die exit revealed that elongated bands contained in the shear and transition zone flow into the subsurface regions of the extrudate during steady state extrusion further confirming the occurrence of grains "leaking" from the dead metal zone into the surface of the extrudate [10, 12]. This grain "leakage" from the dead metal zone during indirect extrusion could provide the grain assembly for the formation of PCG at the surface of extrudates as was described in previous work [27].

4.2 Extrudate Microstructure

Extrudate microstructures were studied to analyze the effect of cooling rate on PCG depth. Investigation of extrudate surface structures at both the die exit and steady state regions confirm previous research stating that a PCG structure results from a static recrystallization process [12]. Previous work utilized a forced air quench on extrudates, whereas, a water spray quench was utilized in the current work. This improvement in quenching from previous conditions allowed for a better representation of the actual deformed microstructure immediately after extrusion. Therefore, it has been further determined by this work that immediate quenching of extrudates with water is crucial to reducing PCG depths on the surface of 6061

extrudates. Extrudate surfaces containing no PCG structure further confirmed the possibility of fine, equiaxed, high-angle grains "leaking" from the dead metal zone into the extrudate surface as surface grains strongly resemble those found in the dead metal zone of all partially extruded billets. PCG depths were found to increase with increasing extrusion ratio and ram speed similar to previously reported results.

4.3 Experimental Techniques for Metal Flow Characterization within a Partially Extruded Billet

Characterization of both the metal flow and microstructure within indirect partially extruded billets required the investigation of numerous analytical methods. Traditionally, flow patterns and billet microstructures have been studied with physical modeling, LOM, and Transmission Electron Microscopy (TEM) [5, 10, 28, 29]. The research presented in this thesis; however, suggests that these traditional methods fail to represent the metal flow at the meso-scale. For example, use of LOM in this research to determine dead metal zone depths proved to be subjective and inaccurate as the microstructure within the dead metal zone was not resolvable. General metal flow patterns, conversely, could be deduced from LOM; however, physical relationships regarding the effect of process parameters on billet evolution could not be precisely determined solely by LOM as seen in Figures 44 and 45. Failure of LOM to accurately present the microstructure and transitions between deformation zones demanded the use of EBSD within the current work.

Using EBSD, various methods to understand and define the dead metal/shear zone transition were utilized. EBSD was useful in providing the meso-scale information needed to understand the microstructural and physical features that occur during the extrusion process. Grain shape aspect ratio measurements, as seen in Figure 47, contained excessive scatter as fine, equiaxed grains were present throughout the scanned area and a clear dead metal zone/shear zone interface was not found using this method. Again, this method proved to be inaccurate in determining and identifying a transition zone between dead metal and shear grains.

The inaccuracy of LOM and certain EBSD techniques led to the use of the grain size method to determine dead metal zone geometry and further understand the dead metal/shear zone interface. Grain size maps obtained from EBSD provided an improved visualization of the diffuse transition from dead metal to shear grains allowing measurements to be taken of the approximate depths of the dead metal zones. Measurements taken using the grain size method; however, still proved tedious as the ambiguity surrounding the transition zone made it difficult to assign an abrupt interface to the transition from the dead metal zone to the shear zone.

4.4 Dead Metal Zone Geometry

The results from dead metal zone geometry measurements using grain size maps reveal that as extrusion progresses the area of dead metal increases in size from

25-75%. It is expected that at the commencement of indirect extrusion the original cast, homogenized grains directly at the die face remain stationary due to friction. It may be theorized that, as extrusion progresses, the dead metal zone increases until it reaches some steady state value. This possible steady state condition for dead metal zone formation may be analogous to that of the extrudate as steady state extrudate microstructures are dictated by the metal flow within the billet. This effect can be seen with the 50% and 75% partially extruded billet LOM micrographs as very little difference was witnessed between them. The 25% sample, however, was just reaching steady state as seen in earlier results.

Due to the symmetry in metal flow patterns witnessed in all partially extruded billets, it is assumed that variations in dead metal zone area witnessed in two dimensions is representative of the volume increase in three dimensions. Therefore, phenomenologically, the volume increase of dead metal is proposed to result from the continuing fragmentation and formation of new high angle grains at the dead metal/shear zone interface. As original grains continue to deform around pre-existing dead zones, grains will continue to thin until impingement and new grain formation occurs causing an accumulation of fine, equiaxed, high angle grains at this interface. As stated above, this process of accumulation will continue until some steady state is achieved within the billet.

Results obtained from dead metal zone geometry measurements, specifically equations describing the geometry and the corresponding areas, will assist in the future development of constitutive equations to be used in numerical modeling of the

indirect extrusion process. To correctly model this process, future work will need to be performed to understand the microstructural and metal flow evolution at both the beginning and end of the extrusion process.

5.0 CONCLUSIONS

The work presented in this thesis has characterized billet evolution, specifically, metal flow and microstructure development, during the indirect extrusion of 6061 aluminum. The following conclusions can be deduced from the current work:

- The Electron Backscatter Diffraction (EBSD) technique proved to be the most useful tool in understanding microstructural development and metal flow of 6061 aluminum billets on the meso-scale.
- Obtaining grain size maps from EBSD data using OIM software proved to be the ideal method for measuring dead metal zone depths among partially extruded billets and understanding the transition from dead metal to deformed grains.
- There exists within a diffuse transition zone separating "continuous" dead metal from the shear zone indirectly extruded billets. The location of this zone among the samples studied varies as both extrusion progresses and the area of dead metal increases.
- The area traditionally known as the dead metal zone during indirect extrusion increases in volume from 25%-75% completion. This increase in volume is attributed to the continuing fragmentation and formation of new, high-angle, fine, equiaxed grains at the dead metal/shear zone interface.

- Fine equiaxed high-angle grains found within the dead metal zone of partially extruded billets likely results from a continuous dynamic recrystallization process such as geometric dynamic recrystallization as evidence of grain fragmentation, formation, and grain boundary serrations does exist within partially extruded billets. These microstructural features are normally associated with a continuously formed microstructure during deformation.
- An improved quenching technique during extrusion eliminates PCG structure formation immediately at the die orifice. PCG formation witnessed in steady state extrudates is concluded to result from static recrystallization.

6.0 FUTURE WORK

Complete understanding of the formation of dead metal zone grains requires knowledge of early deformation stages in the extrusion process. It was not possible to obtain partially extruded billets representing the early stages of indirect extrusion (<25% completion) with the small scale extrusion press used in this research. Future work; however, should investigate the earlier stages of extrusion specifically prior to steady state to further understand the formation of dead metal zone grains. As stated before, work also needs to be performed to investigate the effect of extrusion testing parameters on dead metal zone geometry and area. Information gained from the current and future work will aid in the development of finite element models (FEM) to correlate microstructural data with deformation parameters. Overall, research in this area may help further explain the variation in PCG depths witnessed in extrudates of varying testing conditions.

Also, complete understanding of the recrystallization processes that occur in the billet at the billet/die interface requires TEM characterization of this region. TEM will provide useful knowledge as to the substructure development during the extrusion process. Once full knowledge is obtained about the structure development within the billet during the extrusion process an adequate model of metal flow into the extrudate surface during indirect extrusion could be obtained.

Since the overall goal of this work was to understand billet evolution in reference to extrudate surface structure, the knowledge gained from this work should be extended to the direct extrusion process and eventually to an industrial scale.

7.0 REFERENCES

1. Association, T.A., *Aluminum Standards and Data.* 1997. p. 1-9, 2-13.

2. Saha, P.K., *Aluminum Extrusion Technology.* 2000, Materials Park, OH: ASM International.

3. Anderson, A.N. *Physical Metallurgy and Extrusion of 6063 Alloy.* Proceedings of *5th International Aluminum Extrusion Technology Seminar*, 1992, The Aluminum Association, Chicago, IL, Vol. I, 43-56.

4. Dieter, G.E., *Mechanical Metallurgy.* 3rd ed. Materials Science and Engineering, ed. R. Gibala, M. Tirrell, and C. Wert. 1986, New York: McGraw-Hill, Inc.

5. Valberg, H. *Physical Simulation of Metal Extrusion by Means of Model Materials.* Proceedings of *Fourth International Aluminum Extrusion Technology Seminar*, 1988, The Aluminum Association and Aluminum Extruders Council, Chicago, Il, Vol. II, 321-327.

6. Laue, K. and H. Stenger, *Extrusion.* 2nd ed. 1981, Metals Park, Ohio: ASM. 457.

7. Bandar, A., et al. *Physical and Numerical Modeling of Billet Upsetting.* Proceedings of *Seventh International Aluminum Extrusion Technology Seminar*, 2000, The Aluminum Association and Aluminum Extruders Council, Chicago, Il, Vol. I, 159-166.

8. Bandar, A., K. Lorcharoensery, and W.Z. Misiolek, *Three-dimensional material flow analysis of asymmetric hollow extrusions.* Journal of Materials Processing Technology, 1998(80-81): p. 657-664.

9. Durrschnabel, W., *Der Materialfluss beim Strangpressen von NE-metallen.* Metall, 1968. **22**: p. 426-437.

10. Valberg, H. *A Modified Classification System for Metal Flow Adapted to Unlubricated Hot Extrusion of Aluminum and Aluminum Alloys.* Proceedings of *5th International Aluminum Extrusion Technology Seminar*, 1996, Vol. I, 95-100.

11. Misiolek, W.Z. and R.M. Kelly. *Dead Metal Zones in Extrusion of Complex Shapes*. Proceedings of *5th International Aluminum Extrusion Technology Seminar*, 1992, The Aluminum Association and Aluminum Extruders Council, Chicago, IL, Vol. I, 315-318.

12. Van Geertruyden, W.H., W.Z. Misiolek, and P.T. Wang. *Analysis of Peripheral Coarse Grain Recrystallization in 6xxx Aluminum Alloy Extrusion*. Proceedings of *Eighth International Aluminum Extrusion Technology Seminar*, 2004, Orlando, FL, (In Press)

13. Walters, V.R. *Recent Developments in Intermediate and High Strength 6xxx Series Alloys*. Proceedings of *ET'84: Extrusion Productivity Through Automation*, 1984, The Aluminum Association, Atlanta, GA, Vol. I, 75-80.

14. Hatch, J., *Aluminum: Properties and Physical Metallurgy*. 1984, Metals Park, OH: ASM.

15. Sperry, P. *Correlation of Microstructure in 6xxx Extrusion Alloys With Process Variables and Properties*. Proceedings of *ET'84: Extrusion Productivity Through Automation*, 1984, The Aluminum Association, Vol. I, 21-29.

16. Beatty, B.C. *How Billet Structures Affect Extrusion Performance of 6061 Alloy*. Proceedings of *Second International Aluminum Extrusion Technology Seminar*, 1977, Aluminum Extruders Council and The Aluminum Association, Vol. 1, 225-228.

17. Polmear, I.J., *Light Alloys*. 1995: Halstead Press.
18. Humphreys, F.J. and M. Hatherly, *Recrystallization and Related Annealing Phenomena*. First ed. 1995, Oxford: Pergamon. 497.

19. Doherty, R.D., et al., *Current issues in recrystallization: a review*. Materials Science and Engineering A, 1997. **238**: p. 219-274.

20. Blum, W. and H.J. McQueen, *Dynamics of Recovery and Recrystallization*. Materials Science Forum, 1996. **217-222**: p. 31-42.

21. Hughes, D.A., et al., *Scaling of Misorientation Angle Distributions*. Physical Review Letters, 1998. **81**(21): p. 4664-4667.

22. Gourdet, S. and F. Montheillet, *An experimental study of the recrystallization mechanism during hot deformation of aluminum*. Materials Science and Engineering A, 2000. **283**: p. 274-288.

23. Blum, W., et al., *Geometric dynamic recrystallization in hot torsion of Al-5Mg-.6Mn (AA5083).* Materials Science and Engineering A, 1996. **205**: p. 23-30.

24. Gourdet, S., et al., *Recrystallization during hot deformation of Aluminum.* Materials Science Forum, 1996. **217-222**: p. 441-446.

25. Konopleva, E.V., H.J. McQueen, and E. Evangelista, *Serrated Grain Boundaries in Hot-Worked Aluminum Alloys at High Strains.* Materials Characterization, 1995. **34**: p. 251-264.

26. McQueen, H.J. and W. Blum, *Dynamic recovery: sufficient mechanism in the hot deformation of Al (<99.99).* Materials Science and Engineering A, 2000. **290**: p. 95-107.

27. Van Geertruyden, W.H., *The Origin of Surface Recrystallization of 6xxx Aluminum Alloys*, in *Ph.D. Dissertation*. 2004, Lehigh University: Bethlehem, PA.

28. Bandar, A., et al. *Improving flow in soft-core bimaterial billets.* Proceedings of *Seventh International Aluminum Extrusion Technology Seminar*, 2000, The Aluminum Association and Aluminum Extruders Council, Chicago, IL, Vol. I,

29. Clode, M.P. *Material Flow and Microstructural Development During Extrusion of AA6063.* Proceedings of *Fifth International Aluminum Extrusion Technology Seminar*, 1992, The Aluminum Association and Aluminum Extruders Council, Chicago, IL, Vol. II, 79-99.

VITA

Heather M. Browne was born on November 19, 1980 to parents Deborah L. and John J. Browne in Philadelphia, PA. Heather first attended Holy Cross Elementary School in Springfield, PA then Upper Darby High School in Upper Darby, PA. After graduating Upper Darby in 1998, Heather entered Lehigh University in the fall of 1998 and graduated with a Bachelor's of Science in Materials Science and Engineering in 2002. Heather entered graduate studies at Lehigh University in June of 2002 in pursuit of a Master of Science degree also in Materials Science and Engineering. During her graduate career, Heather was the first Extrusion Technology for Aluminum Profiles Foundation Graduate Fellow, authored one conference paper, and was the winner of both the Association of Women in Science Robert E. Davies award and International Aluminum Extrusion Design competition.

END OF TITLE